MICROSTRUCTURAL AND BIOLOGICAL PROPERTIES OF DICALCIUM PHOSPHATE/CALCIUM SILICATE HYDRATE CEMENT COMPOSITES FOR ORTHOPEDIC APPLICATIONS

2024
MASTER THESIS
BIOMEDICAL ENGINEERING

Mohamed ALHELEBU

Thesis Advisors
Assoc. Prof. Dr. Daver ALI
Assist. Prof. Dr. Ammar ZIDANOĞLU

MICROSTRUCTURAL AND BIOLOGICAL PROPERTIES OF DICALCIUM PHOSPHATE/CALCIUM SILICATE HYDRATE CEMENT COMPOSITES FOR ORTHOPEDIC APPLICATIONS

Mohamed ALHELBU

Thesis Advisors
Assoc. Prof. Dr. Daver ALI
Assist. Prof. Dr. Ammar ZIDANOĞLU

T.C.
Karabuk University
Institute of Graduate Programs
Department of Biomedical Engineering
Prepared as
Master Thesis

KARABÜK
June 2024

I certify that in my opinion the thesis submitted by Mohamed ALHELEBU titled "MICROSTRUCTURAL AND BIOLOGICAL PROPERTIES OF DICALCIUM PHOSPHATE/CALCIUM SILICATE HYDRATE CEMENT COMPOSITES FOR ORTHOPEDIC APPLICATIONS" is fully adequate in scope and in quality as a thesis for the degree of Master of Science.

Assoc. Prof. Dr. Daver ALI .....
Thesis Advisor, Department of Biomedical Engineering

Assist. Prof. Dr. Ammar ZIDANOGLU .....
2. Thesis Advisor, Department of Biomedical Engineering

This thesis is accepted by the examining committee with a unanimous vote in the Department of Biomedical Engineering as a Master of Science thesis. June 21, 2024

Examining Committee Members (institutions) Signature

Chairman : Assist. Prof. Dr. İsmail Seçkin ÇARDAKLI (ATAU) .....

Member : Assoc. Prof. Dr. Daver ALI (KBU) .....

Member : Assist. Prof. Dr. Khaled M.N. CHAHROUR (KBU) .....

The degree of Master of Science by the thesis submitted is approved by the Administrative Board of the İnstitute of Graduate Programs, Karabuk University.

Assoc. Prof. Dr. Zeynep ÖZCAN .....
Director of The Graduate Education Institute

"I hereby declare that all information in this document has been obtained and presented in accordance with academic rules and ethical conduct. I also declare that, as required by these rules and conduct, I have fully cited and referenced all material and results that are not original to this document."

Mohamed ALHELEBU

ABSTRACT

M. Sc. Thesis

MICROSTRUCTURAL AND BIOLOGICAL PROPERTIES OF DICALCIUM PHOSPHATE/CALCIUM SILICATE HYDRATE CEMENT COMPOSITES FOR ORTHOPEDIC APPLICATIONS

Mohamed ALHELEBU

Karabuk University
Institute of Graduate Programs
Department of Biomedical Engineering

Thesis Advisors:
Assoc. Prof. Dr. Daver ALI
Assist. Prof. Dr . Ammar ZIDANOGLU
June 2024, 59 pages

This study investigates the microstructural and biological properties of calcium silicate hydrate (CSH) cement composites modified with varying dicalcium phosphate (DCP) fractions. The primary objective is to enhance the biocompatibility and antibacterial properties of CSH cement for potential orthopedic and dental applications. The research involved synthesizing β-dicalcium silicate (β-C_2S) using the sol-gel method and preparing CSH cement with 20%, 30%, and 40% DCP additions. Microstructural characterization was performed using X-ray diffraction (XRD), Fourier-transform infrared spectroscopy (FTIR), and scanning electron microscopy (SEM). The XRD analysis revealed decreased crystallinity and particle size with increasing DCP content. The FTIR spectra confirmed the presence of

characteristic peaks for both CSH and DCP, indicating the successful incorporation of DCP into the cement matrix. SEM images showed a highly interconnected structure with reduced pore size as the DCP content increased. Thermogravimetric analysis (TGA) demonstrated that all cement samples maintained stability at temperatures up to 700°C, with weight loss percentages of 26.048% for pure CSH, 20.631% for 20% DCP/CSH, 16.662% for 30% DCP/ CSH, and 10.539% for 40% DCP/ CSH. The antibacterial efficacy against Staphylococcus aureus (*S. aureus*) was highest at 200 mg/ml concentration for pure CSH loaded with gentamicin, with reduced efficacy observed as DCP content increased. Biocompatibility tests using Osteosarcoma (Saos-2) cells indicated a significant reduction in cell viability with pure CSH cement, which was improved by adding DCP. Specifically, cell viability was 81.24% on day 1, 65.32% on day 4, and 53.19% on day 7 for pure CSH, while 20% DCP/CSH showed 78.96% on day 1, 41.86% on day 4, and 26.26% on day 7. These findings suggest that incorporating DCP into CSH cement enhances its microstructural properties, thermal stability, and biocompatibility, making it a promising candidate for bone repair applications.

Key words : β-Dicalcium silicate, Dicalcium phosphate, Characterizations, antibacterial activity; Cell culture analysis.

Science Code **:** 92503.

ÖZET

Yüksek Lisans Tezi

ORTOPEDİK UYGULAMALAR İÇİN DİKALSİYUM FOSFAT/KALSİYUM SİLİKAT HİDRAT ÇİMENTO KOMPOZİTLERİNİN MİKRO YAPISAL VE BİYOLOJİK ÖZELLİKLERİ

Mohamed ALHELEBU

Karabük Üniversitesi
Lisansüstü Eğitim Enstitüsü
Biyomedikal Mühendisliği Anabilim Dalı

Tez Danışmanları:
Doç.Dr. Daver ALI
Dr. Öğr. Üyesi . Ammar ZIDANOGLU
Haziran 2024, 59 sayfa

Bu çalışmada, farklı dikalsiyum fosfat (DCP) fraksiyonları ile modifiye edilmiş kalsiyum silikat hidrat (CSH) çimento kompozitlerinin mikro yapısal ve biyolojik özellikleri araştırılmıştır. Birincil amaç, potansiyel ortopedik ve dental uygulamalar için CSH çimentosunun biyouyumluluğunu ve antibakteriyel özelliklerini geliştirmektir. Çalışmada, sol-jel yöntemi kullanılarak β-dikalsiyum silikat (β-C_2S) sentezlenip ve %20, %30 ve %40 DCP ilave ederek CSH çimentosu hazırlanmıştır. Mikro yapısal karakterizasyon, X-ışını kırınımı (XRD), Fourier dönüşümlü kızılötesi spektroskopisi (FTIR) ve taramalı elektron mikroskobu (SEM) kullanılarak gerçekleştirildi. XRD analizi, artan DCP içeriğiyle birlikte azalan kristallik ve parçacık boyutunu gösterdi. FTIR spektrumları, hem CSH hem de DCP için karakteristik piklerin varlığını doğruladı ve DCP'nin çimento matrisine başarılı bir

şekilde dahil edildiğini gösterdi. SEM görüntüleri, DCP içeriği arttıkça gözenek boyutunun küçülmesine rağmen büyük oranda birbirine bağlı gözenekli yapıya sahip olduğunu gösterdi. Termogravimetrik analiz (TGA), tüm çimento numunelerinin 700°C'ye kadar sıcaklıklarda kararlılığını koruduğunu, saf CSH için %26,048, %20 DCP/CSH için %20,631, %30 DCP/CSH için %16,662 ve %40 DCP/CSH için %10,539 ağırlık kaybı gösterdi. Staphylococcus aureus'a karşı antibakteriyel etkinlik, gentamisin içerikli saf CSH için 200 mg/ml konsantrasyonda en yüksekti ve DCP içeriği arttıkça etkinliğin azaldığı gözlemlendi. Osteosarkoma (Saos-2) hücreleri kullanılarak yapılan biyouyumluluk testleri, saf CSH çimentosu ile hücre canlılığında önemli bir azalma olduğunu ve bunun DCP eklenmesiyle iyileştiğini gösterdi. Saf CSH için hücre canlılığı 1. günde %81,24, 4. günde %65,32 ve 7. günde %53,19 iken, %20 DCP/CSH 1. günde %78,96, 4. günde %41,86 ve 7. günde %26,26 olarak saptanmıştır. Bu bulgular, DCP'nin CSH çimentosuna dahil edilmesinin mikro yapısal özelliklerini, termal stabilitesini ve biyouyumluluğunu artırdığını ve onu kemik onarım uygulamaları için umut verici bir malzeme olduğunu göstermektedir.

Anahtar Kelimeler : β-Dikalsiyum silikat, Dikalsiyum fosfat, Karakterizasyonlar, Antibakteriyel aktivite, Hücre kültürü analizi.

Bilim kodu **:** 92503

ACKNOWLEDGEMENT

I wish to extend my heartfelt appreciation to Assist. Prof. Dr . Ammar ZIDANOGLU Thank you for approving my application to work under his guidance and for your unwavering support, timely interventions, and invaluable advice during my project, which significantly contributed to its successful completion. His approachable manner and mentorship greatly facilitated effective communication and collaboration. Additionally, I would like to express my sincere gratitude and appreciation to Assoc. Prof. Dr. Daver ALI, thank you for your guidance, support, and patience while completing this work. Additionally, I am grateful to Assist. Prof. Dr. Ali Deniz DALGIÇ, thank you for your valuable assistance throughout this endeavour.

I express profound gratitude to my parents for their unwavering support and invaluable contributions throughout my academic journey and this research endeavour. Additionally, heartfelt thanks are extended to my siblings for their significant encouragement during my thesis research.

CONTENTS

Page

Page

Page

LIST OF FIGURES

Page

LIST OF TABLES

Page

SYMBOLS AND ABBREVIATIONS

SYMBOLS

°	: Degree.
°C	: The degree Celsius.
Å	: Angstrom.
cm	: Centimeter.
eV	: Electronvolt.
g	: Gram.
h	: Hour.
min	: minute.
mL	: milliliter.
nm	: Nanometer.
ppm	: parts pert million.
α	: Alpha, cell angle.
β	: Beta, cell angle.
γ	: Gamma, cell angle.
2θ	: The diffraction angle.

ABBREVIATIONS

β-C_2S	: β-Dicalcium Silicate.
C	: Carbon.
Ca	: Calcium.
CS	: Calcium silicate.
C_2S	: Dicalcium Silicate.
C_3S	: Tricalcium Silicate.
$Ca(OH)_2$	: Calcium Hydroxide.
CSD	: The critical sized defect.
DCP	: Dicalcium Phosphate.
DCPA	: Anhydrous Dicalcium Phosphate.
FTIR	: Fourier transform infrared.
JCPDS	: Joint Committee on Powder Diffraction and Standards.
HA	: Hydroxyapatite.
MCS	: monocalcium silicate.
MTA	: mineral trioxide aggregate.
P	: phosphorus.
Si	: Silicon.
SPS	: Spark Plasma Sintering.
SEM	: Scanning Electron Microscopy.
TCP	: Tricalcium phosphate.
TEM	: Transmission electron microscopy.
XRD	: X-ray diffraction.

CHAPTER 1

INTRODUCTION

1.1.STRUCTURE AND DEVELOPMENT OF BONES

Bone is a complex substance characterized by its layered composition, which has attracted biologists' attention due to its vital physiological role. It has also intrigued materials engineering specialists because of its unique structure and mechanical properties [1]. Bone comprises various structural elements of varying sizes that perform various mechanical, biological, and chemical functions. These include structural stability, the protection and retention of regenerative cells, and the maintenance of mineral balance in the form of ions [2]. Figure 1.1 categorizes bone structure into two distinct types based on its arrangement: The compact bone is characterized by a relatively small outer surface area that encloses the inner medullary cavity. Spongy or cancellous bone, also called cancellous bone, exhibits a reduced density and an increased surface area compared to compact bone. Approximately 80% of the skeletal structure comprises compact bone, while the distal sections of long bones, vertebral bodies, and the calcaneum consist mainly of spongy bone. In contrast, compact bone is predominantly found in the shafts of long bones and the femoral neck [3].

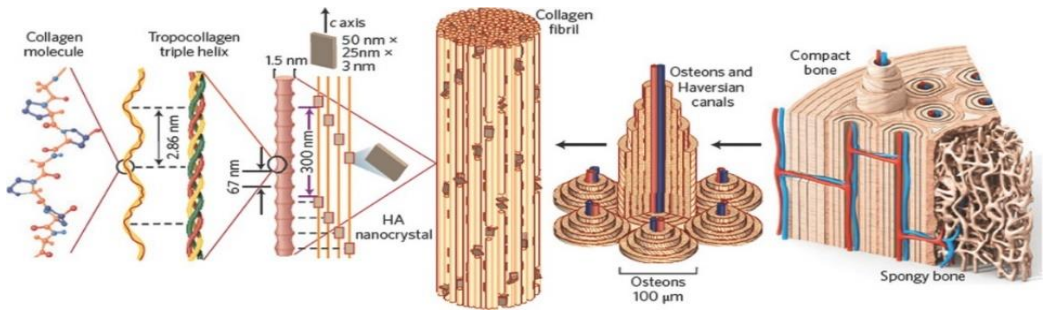

Figure 1.1. Diagram showing how bone is arranged structurally at all scales, from macroscopic to nanoscale [4].

Osteons and trabecular packets, recurring microscopic units, make up every structure. The structural components of these building blocks consist of mineralized collagen fibres arranged in layers known as lamellae. The formation of these fibres occurs at a minuscule level, originating from collagen fibrils of even smaller dimensions. These collagen fibrils, in turn, comprise collagen molecules that bear hydroxyapatite crystals [5].

1.2.CEMENT AS A BONE-RESTORAION MATERIAL

Bone possesses remarkable regeneratIve capabilities and can undergo self-healing processes, provided that the injury does not exceed a threshold known as the "critical size defect." In such cases, the newly generated bone resembles bone that has not been damaged. The critical-sized defect (CSD) refers to the specific threshold beyond which bone fractures are unable to undergo spontaneous regeneration [6]. In this manner, comprehensive examinations of bone repair methodologies have been recorded. These include autografts, which involve grafts sourced from the same individual; allografts, which involve grafts from different individuals of the same species; and transplants sourced from both the recipient and others [7]. Autografts are widely recognized as the benchmark in bone repair within the academic community [8]. These substances possess critical components necessary for optimal bone functionality, bone tissue development, and bone growth promotion while mitigating the risk of immune reactions through tissue compatibility.

Nevertheless, the utilization of autografts in transplantation procedures is a costly approach that is accompanied by considerable detrimental effects at the site of donor extraction [9]. Additionally, there are potential concerns about ailments, impairments, scarring, and surgical risks, including bleeding, inflammation, infection, and enduring discomfort [10]. Due to the limitations associated with bone grafts derived from human sources, researchers have redirected their attention toward synthetic materials [11]. Materials technology has witnessed notable progress recently, leading to the emergence of highly advanced materials. Additionally, using tissue engineering methodologies, synthetic compounds have been restructured into complex configurations, incorporating growth-promoting elements and the incorporation of the

patient's stem cells. The objective of this procedure is to establish a technique for the regeneration of bones [12]. Various synthetic alternatives, including biometallics, polymers, bioceramics, and cements, have been suggested and advanced as potential substitutes for natural bone [11,13,14]. Ceramics incorporating calcium phosphate and calcium sulphate have garnered significant interest due to their resemblance to bone minerals. Using ceramics in block or granule configurations encounters difficulty addressing bone injuries with uneven sizes. However, injectable bone cement presents a promising alternative for treating bone defects [15]. Various materials are employed as bone cement, such as β-Dicalcium silicate (β-Ca_2SiO_4, β-C_2S), dicalcium phosphate ($CaHPO_4$, DCP), and Polymethyl methacrylate (PMMA) cement. In orthopedics, PMMA is one of the most widely used polymeric compounds. There are several ways to modify this chemical, which comprises synthetic organic and inorganic components and is regarded as the gold standard in joint replacement surgery. Its ideal qualities, such as non-toxicity and user-friendliness, are credited with its widespread use [16,17]. Joint and spine surgery employs PMMA bone cement due to its biocompatibility [18]. However, because of PMMA's low bioactivity, the primary issue with implants is loosening over long-term use in a physiological environment. PMMA bone cement, like most biomaterials, has several disadvantages that can impact its long-term performance in a physiological environment. Its primary limitation is low bioactivity, which can lead to implant loosening over time. Other significant drawbacks include its failure to bond directly to bone, the high exothermic temperature during the curing process, inertness (lack of biological activity), toxicity from residual monomer, and relatively low mechanical strength compared to natural bone [19,20]. In vivo, these characteristics may result in significant complications such as implant loosening, bone resorption, and necrosis of the surrounding tissues. These issues can compromise the long-term success of implants and may necessitate revision surgeries, highlighting the need for continued research and development in bone cement technology [19–21].

1.2.1. β-Dicalcium Silicate

β-C_2S is important in applications such as Portland cement, refractory materials, and endodontic cement MTA (mineral trioxide aggregate). The compound above exhibits an increased sealing capacity and compatibility with conventional dental materials.

The hydraulic properties of β-C_2S have been confirmed, indicating its ability to interact with water or liquid solutions at typical or physiological temperatures, forming injectable pastes [22]. A group of researchers has successfully formulated a bone cement composed of calcium silicate that exhibits rapid hardening properties. When this cement is combined with a phosphate solution, it shows a significantly heightened reactivity within biological environments, thereby facilitating the proliferation of new bone tissue. The recent discovery has opened up new prospects in naturally solidifying bone repair and augmentation materials. Moreover, the cement's performance attributes, including its solidification and strength rate, substantially influence its efficacy in practical medical contexts [23]. Furthermore, the release of calcium and silicon has the potential to facilitate cellular growth and differentiation in terms of bone health maintenance [24].

1.2.2. Dicalcium Phosphate

DCP is a widely recognized form of bone cement, increasingly recognized for its notable characteristics and diverse applications across various disciplines. The utilization of this technology spans diverse medical disciplines, encompassing orthopedics, pharmaceutical administration, oncology therapy, biological detection, and surgical interventions in the skull and facial regions. It is worth mentioning that a substantial decrease in heat release was observed during the setting process of dicalcium phosphate cement. DCP exhibits potential as a viable alternative for bone grafting, specifically for minor bone injuries, and a substitute for load-bearing prosthetic implants [25,26]. Over the last two decades, researchers have conducted extensive research to improve the physical properties, solidification duration, application, and biocompatibility of DCP cements. The precise timing of bone cement solidification is important in clinical applications, particularly in minimally invasive procedures. The rate at which the cement undergoes hardening should be optimal, striking a balance between being neither excessively rapid nor excessively slow to facilitate surgeons' smooth execution of surgical procedures. Surgeons should meticulously choose the appropriate solidification duration to ensure that the cement mixture achieves sufficient structural integrity during solidification. By employing this

approach, it is possible to effectively mitigate the undesired displacement of cement to unfavourable destinations [27].

1.3.PROBLEM STATEMENT

The problem statement for this research addresses the limitations of Calcium silicate hydrate (CSH) cement in orthopedic and dental applications. Pure CSH cement exhibits high alkalinity and potential cytotoxicity, which can lead to reduced cell viability and biocompatibility issues. There is a need for materials with both biocompatibility and antibacterial properties to prevent infections in orthopedic and dental procedures. Additionally, there is a lack of understanding about how modifying CSH cement with additives like DCP affects its overall performance and suitability for clinical use. This research aims to address these problems by investigating the effects of incorporating different fractions of DCP into CSH cement to develop an improved composite material that balances biocompatibility, antibacterial properties, and microstructural characteristics for potential use in orthopedic and dental applications, mainly as fillers for bone defects and cavities [28–30].

1.4.OBJECTIVES OF THE THESIS:

The study aims to investigate the effects of incorporating different fractions of DCP (20%, 30%, and 40%) into CSH cement on its microstructural and biological properties. Specifically, the research focuses on:

- Synthesizing β-C_2S as a precursor material to prepare CSH cement by mixing 1 gram of β-C_2S with 0.5 mL of water.
- Characterizing the microstructural changes in CSH cement when different fractions of DCP are added. This includes:
- Examining X-ray diffraction (XRD) patterns to determine crystallinity
- Analyzing Fourier Transform Infrared (FTIR) spectra to identify chemical bonds and functional groups
- Studying Scanning Electron Microscopy (SEM) images to assess particle size and surface morphology of the cement composites

- Analyzing the thermal behavior of pure CSH and DCP-modified CSH cements through thermogravimetric analysis (TGA) to:
- Identify distinct weight loss stages
- Evaluate the impact of DCP on these stages
- Evaluating the antibacterial efficacy of the cement composites loaded with Gentamicin antibiotic against Staphylococcus aureus (*S. aureus*) by:
- Measuring bacterial growth in the presence of the cement samples
- Comparing the antibacterial properties of different DCP concentrations
- Assessing the biocompatibility of the cement composites by evaluating the viability of Osteogenic sarcoma (Saos-2) cells exposed to the cement samples:
- Measuring cell viability over different durations (one day, four days, and seven days)
- Investigating the effect of DCP addition on cell viability compared to pure CSH.

1.5.SIGNIFICANCE OF THE THESIS

DCP/CSH cement development offers significant potential for orthopedic applications. This type of cement is injectable, biocompatible, and resorbable, allowing it to fit tightly to bone defects. It can also be an effective carrier for functional substances in bone tissue treatment, enabling localized drug delivery. This allows for more effective treatment of various bone diseases and defects with minimal side effects compared to systemic therapies. Overall, advancing our understanding and capabilities in cement analysis and bone cement formulation can improve construction materials and orthopedic treatments, with wide-ranging benefits for infrastructure and healthcare
.

CHAPTER 2

LITERATURE REVIEW

2.1. CALCIUM SILICATE

Because silicate-based ceramics have superior bioactivity over calcium phosphate-based ceramics, they have recently attracted a lot of positive attention [31]. Simple Ca-Si bioceramic calcium silicate (CS) has shown biocompatibility, biodegradability, and bioactivity. CS may have excellent potential for bone tissue engineering because of its osteogenic qualities, which encourage the growth and development of osteoblastic cells [32]. One of the primary properties of CS is its ability to stimulate bone-like apatite mineralization in both in vitro and in vivo post-implantation simulated bodily fluid. Because of this characteristic, a robust chemical link is formed at the material-bone contact, which facilitates osteointegration and speeds up the process of bone regeneration [33,34].

Nevertheless, using this substance as a biomaterial is a relatively recent advancement, originating only within the past two decades. Calcium to silicon (Ca/Si) ratios categorize CS into three distinct types. These types include monocalcium silicate ($CaSiO_3$, MCS), dicalcium silicate (Ca_2SiO_4, C_2S), and tricalcium silicate (Ca_3SiO_5, C_3S). Since its discovery in 1971 by Hench and colleagues, Bioglass has been the subject of extensive research. Researchers have explored different types of biomaterials that incorporate CaO-SiO2. Several materials, such as bioactive glasses, apatite-wollastonite AW glass ceramics, and CS cement, have been extensively studied as potential candidates for repairing or substituting hard tissues [35,36]. CS, commonly referred to as Wollastonite, has the ability to facilitate the process of natural bone integration within a biological organism. Wollastonite's biological response triggers the formation of hydroxyapatite (HA) by releasing calcium and silicate ions. It is assumed that this particular

substance possesses the capacity to induce bone growth, offering the supplementary advantage of exhibiting non-toxic properties towards cellular entities [37]. CS is the source of MTA, a self-hardening material with hydraulic properties. These substances primarily consist of dicalcium and tricalcium silicates. Water is a substance that attracts them, and when subjected to X-ray imaging, their appearance is characterized by opaqueness. The characteristics above give rise to the creation of CSH, a cohesive gel that undergoes self-hardening [38].

2.1.1. Monocalcium Silicate (wollastonite)

Wollastonite ($CaSiO_3$) is composed of 48.3% calcium oxide (CaO) and 51.7% silicon dioxide (SiO_2) [39,40]. Wollastonite is so much better at promoting bone repair and regeneration than ceramics consisting of C_2S and C_3S. It has garnered a lot of attention in the field of ceramic materials. The compound under consideration exhibits two discernible structures, namely β-wollastonite (β-$CaSiO_3$) and α-wollastonite (α-$CaSiO_3$) [41]. The former structure is observed to manifest at lower temperatures, while the latter structure is observed to manifest at higher temperatures [42]. The material exhibits diverse characteristics, encompassing elevated thermal resistance, restricted thermal conductivity, resistance to corrosion, inertness towards chemical reactions, and a diminished electrical insulating capacity [43]. Wollastonite has garnered attention as a promising candidate for bone implants due to its advanced bio-functionalities, exceptional capacity to interface with living tissues, and compatibility with the human body [44]. Including calcium and silicon ions in wollastonite highlights their pivotal function in developing a hydroxyapatite coating. The presence of these ions exerts influence on the mineralization process and assumes a substantial function in the mechanism that facilitates bone integration [45]. Wollastonite has six formula units per unit cell and crystallizes in the triclinic system in the space group P1, with lattice constants a=7.94 A, b=7.32 A, and c=7.07 A [46].

Table 2.1. The physical and chemical properties of wollastonite [47].

Description	Value
Color	White
Luster	Vitreous, Pearly
Molecular weight, gmol^{-1}	116
Specific gravity, gcm^{-3}	2.86–3.09
Refractive index	1.63
pH (10% slurry)	9.9
Solubility in water (g/100 cc)	0.0095
Density (g/cm^3)	2.70–3.00
Hardness (Mohs)	4.5–5
Melting point (°C)	1540

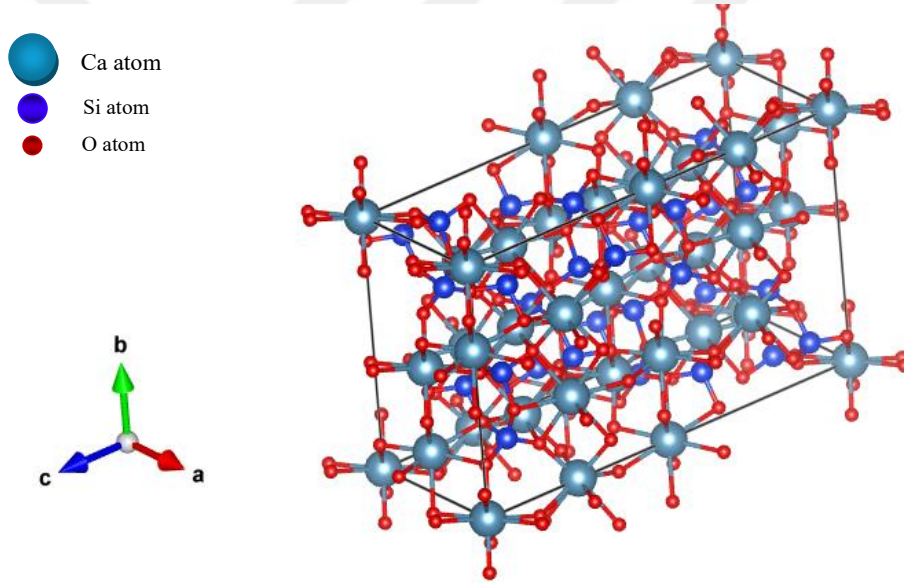

Figure 2.1. The unit cell structure of Monocalcium Silicate (wollastonite).

2.1.2. Dicalcium Silicate:

Dicalcium silicate (Ca_2SiO_4, C_2S) is a critical constituent in Portland cement and plays an important role in the calcium-silicate system. Additionally, it exhibits promising potential in bone defect regeneration [48]. It is a novel bioactive inorganic silicon, calcium, and oxygen compound, including CaO-SiO_2 constituents. The release of silicon ions from the C_2S layer is a significant factor in skeletal development and repair [49]. C_2S is known to exist in five distinct polymorphic forms, namely α, α′H, α′L, β,

and γ. Among these polymorphs, the γ phase is thermodynamically stable at room temperature, while the β phase exhibits the highest reactivity compared to the other polymorphs [50]. Several studies have provided evidence indicating that using Ca2SiO4 powder ceramics and coatings exhibits bioactive properties, rapidly initiating bone-like apatite layer formation on their surface after immersion in simulated body fluid (SBF) [51]. The chemical compound C_2S has hydraulic properties and can react with water or an aqueous solution to make CSH cements, which are the main products of hydration. This process contributes to the inherent self-setting property and subsequent spontaneous enhancement of material strength. The C_2S paste has the potential to be introduced at the site of the defect via injection, thereby circumventing the need for extensive surgical incisions [24].

Additionally, a previous study has demonstrated that Ca_2SiO_4 ceramics exhibit biocompatibility and have the ability to facilitate the adhesion and spreading of mesenchymal stem cells [52]. Although C_2S-based biocements offer good qualities, they are not appropriate for clinical usage due to their excessively long self-setting time and low compressive strength during the initial stages [53]. In order to improve performance, the setting time of C_2S was shortened by using calcium sulphate hemihydrate, which is renowned for solidifying quickly when it comes into contact with water [54], The results showed that a controlled setting time might be achieved by altering the calcium sulphate hemihydrate content. Magnesium phosphate was also added to cement containing C_3S to enhance its setting time and compressive strength [55].

Table 2.2. The physical and chemical properties of β-C_2S [56].

Property	**Description**
Chemical Formula	Ca_2SiO_4
Chemical Classification	Calcium silicate
Appearance	White to grayish powder
Density	~3.2 - 3.4 g/cm³
Solubility	Insoluble in water
Melting Point	~1450 °C
Crystal System	Monoclinic (typical)

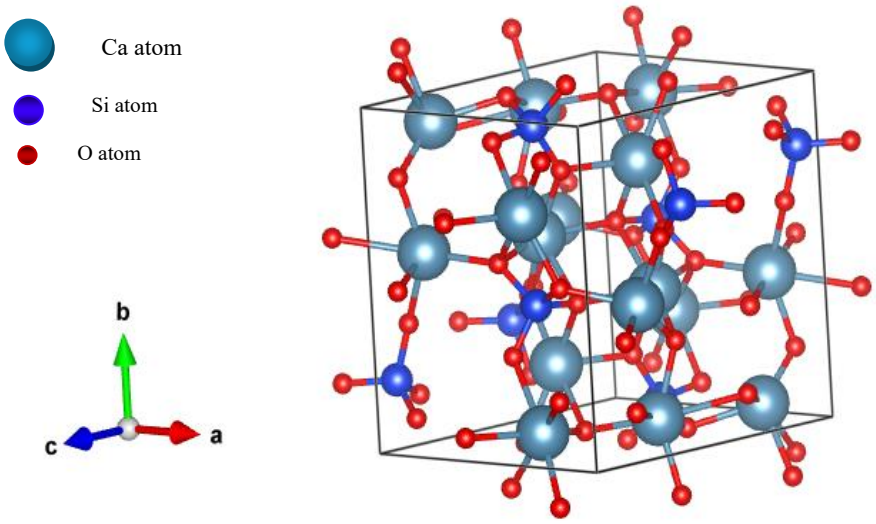

Figure 2.2.The unit cell structure of β-C_2S.

2.1.3. β-Dicalcium Silicate Cement

Calcium silicate bone cement is an innovative injectable biomaterial with unique chemical, biological, and physical characteristics silicate bone cement. Of particular note is the outstanding bioactivity, degradability, and hydration performance of β-C_2S [57]. Despite its potential, its lower compressive strength and excessively fast setting limit its usage in vertebroplasty and kyphoplasty, making it challenging to apply to bone defects with complex structures. Furthermore, the cement's effective clinical applications depend on its physicochemical characteristics, such as compressive strength and setting time [23]. Adding cohesiveness boosters, such as chitosan, gelatin, cellulose, and alginate, to cements improves their characteristics and helps to overcome this constraint [58]. The hydration process of β-C_2S forms $Ca(OH)_2$, which is not normally visible in vivo and significantly deviates from the mineral composition of human bone. In addition, the pH level rises above 12.5 when $Ca(OH)_2$ is present, which harms bone tissue development [59]. More significantly, a rabbit femur model exposed to a 6-month implantation period shows colour stability in a calcium silicate-based cement produced using the sol-gel technique [60]. Human mesenchymal stem

cells can be made to differentiate by the cement even if the growing medium does not contain osteogenic differentiation agents [61].

Table 2.3. CSH's cement physical and chemical properties [62].

Property	Description
Chemical Formula	$Ca_2SiO_4 \cdot xH_2O$ (where x varies)
Chemical Classification	Calcium silicate hydrate
Appearance	White to off-white powder
Density	~2.6 - 2.8 g/cm³
Solubility	Slightly soluble in water
Crystal System	Monoclinic (typical)
Setting Time	Not hydraulic itself

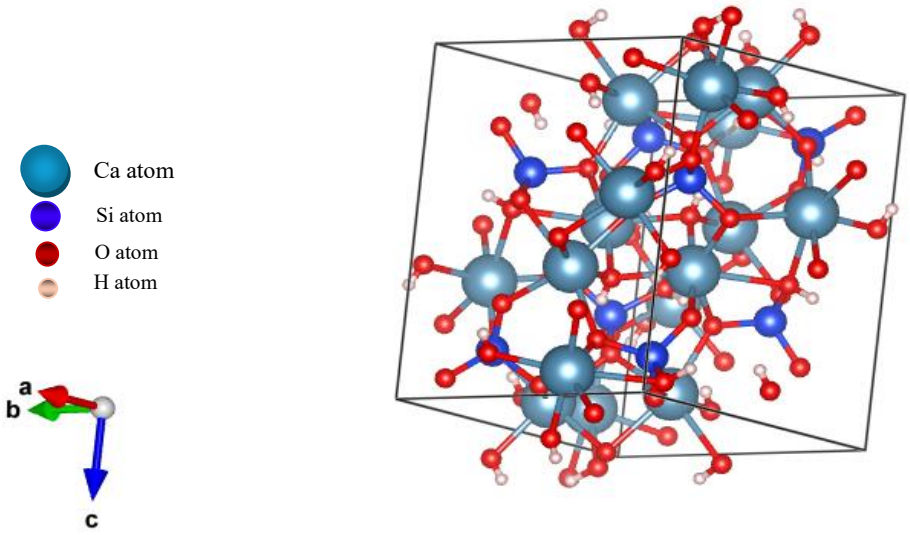

Figure 2.3. The unit cell structure of CSH.

2.1.4. Tricalcium Silicate

Tricalcium silicate (Ca_3SiO_5, C_3S), widely recognized as the primary portland cement component, is extensively utilized in the construction industry. It plays a crucial role in the initial solidification process, encompassing setting time and early mechanical strength, primarily governed by its hydration [63]. The self-setting properties, injectability, moldability, in vitro bioactivity, in vivo biocompatibility, and sustained

drug release capability of (C_3S) bone cement have been extensively demonstrated for bone repair purposes [64]. In vitro, it has the potential to stimulate mineralization resembling bone apatite. The ionic extract solution has the ability to induce the proliferation and osteogenic differentiation of cells related to bone formation, as well as promote the odontogenic differentiation of human dental pulp cells [55]. The primary hydration products of (C_3S) consist predominantly of calcium silicate hydrate (CSH) and calcium hydroxide ($Ca(OH)_2$). The strength and chemical stability of $Ca(OH)_2$ exhibit significant deficiencies. Soft water readily dissolves it, rendering it susceptible to acid corrosion or sulphate attacks. The pH level of cement can reach as high as 12.5 when $Ca(OH)_2$ is present, thereby impeding the growth of additional bone tissue. Calcium oxide (CaO) is a primary constituent in the traditional solid-phase synthesis of (C_3S). To obtain a significantly purer form of C_3S with reduced CaO content, it is necessary to subject the powders to prolonged calcination at elevated temperatures [65,66].

Table 2.4. The Chemical and Physical Properties of C_3S.

Property	**Value**
Chemical Formula	Ca_3SiO_5
Molecular Weight (g/mol)	259.342
CAS Number	1305-78-8
Color	White or grayish-white powder
Solubility in Water	Very low
Melting Point	1450 °C
Density	3.27 g/cm³
Crystal Structure	Triclinic

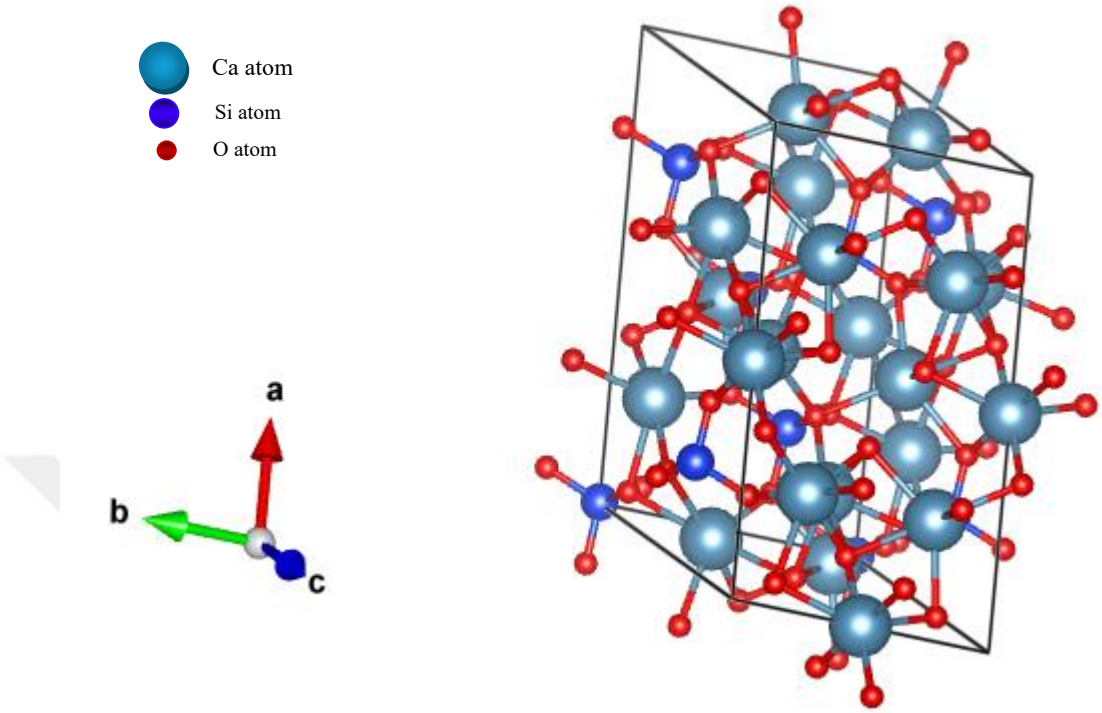

Figure 2.4. The unit cell structure of C_3S.

2.2. DICALCIUM PHOSPHATE

DCP is significant in orthopedics and dentistry due to its calcium phosphate composition, which features a Ca/P ratio 1.0. Moreover, oral hygiene products employ these substances as a dietary supplement and an abrasive agent. Dicalcium phosphate dihydrate (DCPD, $CaHPO_4 \cdot 2H_2O$) and dicalcium phosphate anhydrous (DCPA, $CaHPO_4$) are two commonly employed variants of DCP cement that find extensive applications as substances used for bone fillers. DCPD transforms DCPA when exposed to temperatures of approximately 80ºC [67]. Brushite was synthesized by combining water with a powder composed of acidic calcium phosphate (calcium phosphate monohydrate) and basic calcium phosphate (tricalcium phosphate). This amalgamation resulted in a pliable paste that solidified through an exothermic process, forming a predominantly calcium phosphate dihydrate-based solid. Subsequent investigations demonstrated that brushwood cement exhibited biocompatibility and possessed a distinct advantage compared to other calcium phosphate cement systems,

specifically hydroxyapatite cements. The substance has the ability to reabsorb under physiological conditions. Nevertheless, the initial composition of brush cement yielded a substance that poses challenges in terms of its manipulability, as it solidifies rapidly (within approximately 30 seconds) and exhibits subpar mechanical characteristics (specifically, a radial strength of approximately 1 MPa) [68]. Monetite, also known as anhydrous (DCPA), can be synthesized through two methods. The first method involves adjusting the brush deposition conditions to facilitate the formation of monetite. The second method involves drying a specific brush cement prior to its use. DCPA compound has garnered considerable interest in recent times due to its demonstrated superiority in degradation and regeneration capabilities compared to DCPD. For instance, in vitro assessment has demonstrated that DCPA promotes effective bone resorption and elicits elevated levels of osteogenic gene expression in bone marrow cells compared to (DCPD). According to their findings, DCPA filler has been shown to expedite the process of bone regeneration and achieve a more favorable equilibrium between replacement resorption and the formation of new bone. The degradation of DCPA occurs at a moderate pace, and in contrast to TCP and DCPD, it does not undergo a phase transition to hydroxyapatite (HA) in a physiological setting. The distinctive characteristics of this substance may contribute to its advantageous qualities in relation to resorption and remodeling [69,70].

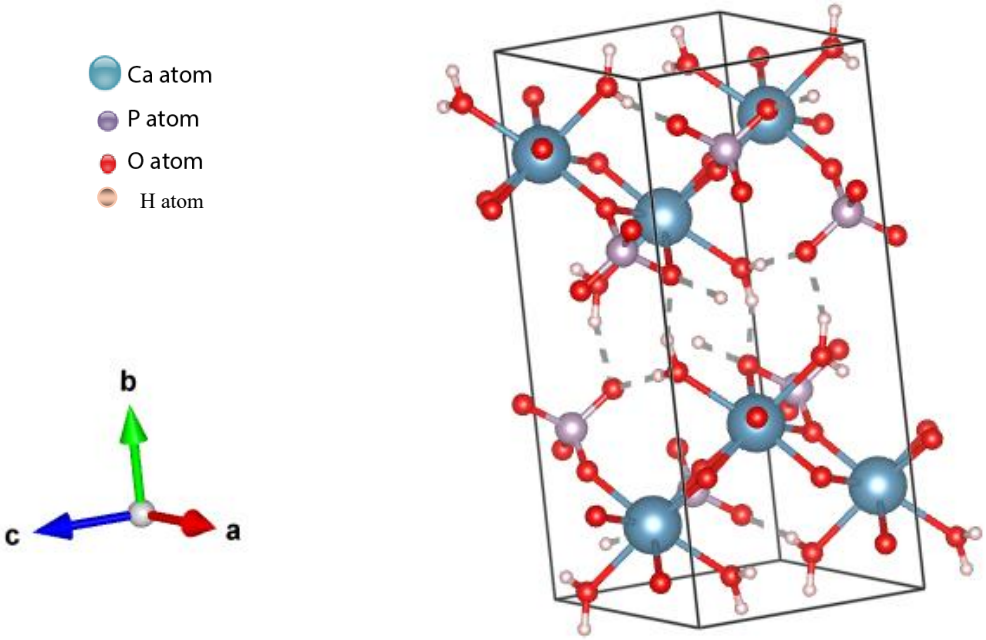

Figure 2.5. The unit cell structure of DCPA.

Table 2.5 Some additives to improve the properties of dicalcium silicate cement.

C_2S	**magnesium (Mg)**	[71]
C_2S	Samarium oxide (Sm^{+3})	[72]
C_2S	borosilicate glass	[73]
C_2S	carboxymethyl cellulose	[74]
C_2S	Chitosan	[23]
C_2S	Gadolinium oxide	[28]

2.3. METHODS TO SYNTHESIZE β-DICALCIUM SILICATE PARTICLES

There are several methods to synthesize β-C_2S particles, each with its own advantages and characteristics:

2.3.1. Hydrothermal Method

This method enables the production of ultrafine and high-purity powders in a relatively brief processing period. The morphology of the materials to be prepared is monitored by employing either low-pressure or high-pressure conditions, depending on the

vapour pressure of the main components involved in the reaction. Hydrothermal synthesis offers notable benefits by effectively mitigating the need for acid and ethanol, owing to the combined influence of elevated temperature and pressure. Furthermore, the hydrothermal method can be employed for green synthesis, eliminating the need for ethanol and acid media. This approach yields calcium silicate powders that exhibit comparable structure and composition to those obtained through the sol-gel route [75,76].

2.3.2. Spark Plasma Sintering

One popular method for quickly densifying different ceramics at room temperature is spark plasma sintering (SPS). The activation of powder particles is thought to be accomplished quickly thanks to applying a high electric-pulsed current during the SPS process, which produces a high heating rate. Grain coarsening can be prevented, and dense ceramics with improved performance can be made using the SPS technique at lower sintering temperatures than conventional sintering techniques because of its high heating rate, high pressure, high-energy activity, and short sintering time [77,78]

2.3.3. Sol-Gel Method

The popular sol-gel techniques are based on the following processes: hydrolysis, polycondensation of nitrates or alkoxides, gelation of colloidal particles, and hypercritical gel drying. After that, the final product is heated to room temperature and dried. β-C_2S with a high specific surface area (up to 26.5–27 m^2/g) and room temperature stability can be synthesized using sol-gel methods, which is an advantage. No additional chemical stabilizers or dopants are needed. In addition, the synthesis temperatures are typically lower than in solid-state synthesis. The small particle size (1-3 μm) of β-C_2S synthesized by the sol-gel method has been suggested as the reason for its stability as it hinders a transformation into γ-C_2S [79,80].

2.3.4. Solid-State Reaction Method

The usual method of obtaining β-C_2S is through solid-state reactions, which involve mixing very fine starter powders (usually $CaCO_3$ and SiO_2) and repeatedly sintering the mixtures at temperatures above 1400°C for several hours. In order to retain the β phase of Ca_2SiO_4, intermediate grinding and the addition of chemical stabilizers are required [50].

Table 2.6 presents a comprehensive comparison of four prominent methods used to prepare (β-C_2S), a crucial component in various cement formulations and biomaterials. This table aims to provide researchers and industry professionals with a clear overview of each method's advantages, disadvantages, and suitability for β-C_2S synthesis.

Table 2.6. Comparison of methods of preparation of β-C_2S.

Method	Advantages	Disadvantages	Suitability for β-C_2S	Reference
Hydrothermal	* Relatively mild conditions * Good control over particle morphology	* Limited control over phase purity * Slower process compared to others * Requires specialized equipment	Can be suitable, but requires optimization to ensure β-C_2S formation. May require post-processing for phase purification.	[81]
Spark Plasma Sintering	* Rapid densification * Achieves high density * Applicable to various materials	* High cost and specialized equipment * May not be ideal for pure β-C_2S synthesis	Not ideal for initial synthesis, but excellent for densification of pre-prepared β-C_2S powder.	[82]
Sol-Gel	*High purity achievable * Good for complex structures	* Time-consuming process * Requires careful control over precursors and processing * Requires specialized equipment and precise control over reaction conditions	A promising method for obtaining pure β-C_2S with tailored properties.	[83]
Solid-State Reaction	* Scalable and cost-effective * Can be used for multi-component materials	* Requires high temperatures and long reaction times * Difficult to achieve high purity	It may be suitable for large-scale production, but achieving pure β-C_2S can be challenging.	[50]

CHAPTER 3

METHODOLOGIES

3.1. MATERIALS

Calcium nitrate tetrahydrate ($Ca(NO_3)_2 \cdot 4H_2O$), tetraethyl orthosilicate ($Si(OC_2H_5)_4$), acetic acid (CH_3COOH), ethanol (C_2H_5OH), di-ammonium hydrogen phosphate ($(NH_4)_2HPO_4$), monocalcium phosphate monohydrate ($Ca(H_2PO_4)_2 \cdot H_2O$), ammonium hydroxide (NH_4OH), and gentamicin sulphate (Merck-Germany) were purchased from Merck, Germany. Dulbecco's Modified Eagle Medium (DMEM), fetal bovine serum (FBS), and penicillin-streptomycin solution were purchased from Biowest, France.

3.2. SAMPLES PREPARATION

3.2.1. Synthesis of β-Dicalcium Silicate Powder

The synthesis of β-C_2S was accomplished using the sol-gel method, employing calcium nitrate tetrahydrate ($Ca(NO_3)_2 \cdot 4H_2O$) and tetraethyl orthosilicate (TEOS) as precursors with a Ca/Si molar ratio of 1.4:1. The process began by solubilizing TEOS in a mixture of ethanol and distilled, deionized water, maintaining a volume ratio of 1:2:4 (water:TEOS: ethanol). After 30 minutes of stirring, 0.5 mL of acetic acid solution was added as a catalyst, and the mixture was stirred for an additional 24 hours to ensure complete TEOS hydrolysis. Subsequently, 1 mole of $Ca(NO_3)_2 \cdot 4H_2O$ was introduced to the hydrolyzed TEOS solution, followed by continuous stirring at 60°C for 6 hours. The solution was left to crystallize at room temperature for 24 hours, forming a hydrogel. The hydrogel was then dried in an oven at 80°C for 48 hours,

producing a xerogel. Finally, the dried gel underwent calcination at 800°C with a heating rate of Coffers advantages such as good homogeneity, high purity, and control over particle size and morphology, making it suitable for various biomaterials and cement chemistry applications. Further characterization using techniques like X-ray diffraction (XRD) and scanning electron microscopy (SEM) could be employed to confirm the formation of the β-C_2S phase and examine its morphological properties [50,84].

3.2.2. Synthesis of β-Tricalcium Phosphate Powder

β-TCP was synthesized using a microwave-assisted wet precipitation method [85]. Two precursor solutions were prepared: solution A containing 42.51 g of $Ca(NO_3)_2 \cdot 4H_2O$ dissolved in 200 mL of distilled water, and solution B containing 15.85 g of $(NH_4)_2HPO_4$ dissolved in 200 mL of distilled water. Both solutions were thoroughly mixed using a magnetic stirrer. Solution B was then gradually added to solution A under constant stirring, with the pH maintained at 7 using ammonium hydroxide. After 30 minutes of stirring at room temperature, the mixture was transferred to a microwave oven and heated at 800 watts for 5 minutes. The resulting precipitate was filtered and washed with distilled water to remove impurities. The sample was then dried overnight in an oven at 80°C. Finally, the dried material underwent calcination at 1000°C for 2 hours to obtain the crystalline β-TCP phase.

3.2.3. Synthesis Of Dicalcium Phosphate/ Calcium Silicate Hydrate Cement Composites

A precise mixture of components was utilized to prepare a pure phase of CSH cement. Initially, 1 gram of β-C_2S was combined with 0.5 grams of distilled water to form the base cement. The experimental procedure was then expanded to include varying proportions of MCPM and β-TCP. These additional components were thoroughly blended with the β-C_2S before introducing water. The water-to-powder ratio was maintained at 0.5 mL per gram of the dry mixture, ensuring consistent hydration across all formulations.

Table 3.1. Weight quantities of reactants used to synthesize pure CSH and DCP/ CSH Cement Composites.

Sample	**Solid Phase (g)**			**Liquid Phase (mL)**
	β-C_2S	β-TCP	MCPM	H_2O
CSH	1	0	0	0.5
20% DCP/ CSH	1	0.133	0.067	0.607
30% DCP/ CSH	1	0.200	0.100	0.660
40% DCP/ CSH	1	0.267	0.133	0.713

3.3. MICROSTRUCTURAL CHARACTERIZATIONS

3.3.1. X-Ray Diffraction

We used the X-ray diffraction (XRD) technique, specifically the Rigaku Ultima IV instrument, to analyze the prepared cement material's phases, network parameters, and purity (Figure 3. 1). In the experiment, the scanning range was defined as spanning from 10 to 90 degrees at a 2θ angle. We set the step size for the scanning process at 0.02 degrees and maintained the scanning speed at one minute per step.

Figure 3.1. XRD device.

3.3.2. Scanning Electron Microscopy

The microstructural analysis of the cement samples was conducted using field emission scanning electron microscopy (FE-SEM), specifically employing a Carl Zeiss Ultra Plus Gemini instrument (Figure 3. 2). This advanced microscopy technique was utilized to examine the particle size distribution and morphology of the cement constituents with high resolution and depth of field. Prior to imaging, the samples were prepared by applying a thin layer of gold coating using a sputter coater. This conductive coating serves multiple purposes: it reduces charging effects, minimizes beam damage to the specimen, and enhances the secondary electron signal, resulting in improved image quality and resolution. The gold coating also helps to lower the spark rate during imaging, which is particularly important for non-conductive materials like cement. FE-SEM imaging allows for the visualization of features at the nanoscale, providing valuable insights into the cement's microstructure, including the size, shape, and arrangement of individual particles and the presence of agglomerates and surface characteristics.

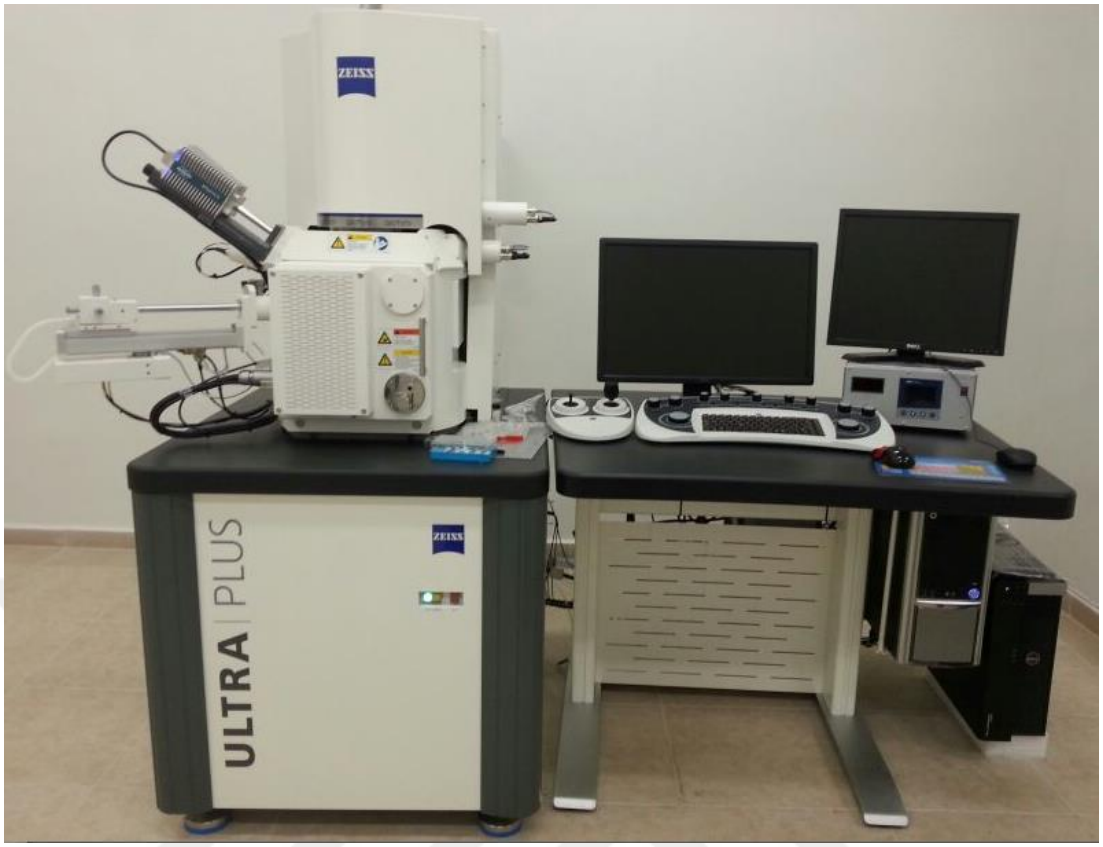

Figure 3.2. SEM device.

3.3.3. Fourier-Transform Infrared Spectroscopy

The presence of functional groups in the cement material was confirmed using Fourier Transform Infrared Spectroscopy (FTIR) with a Perkin Elmer 400 instrument (Figure 3.3). This analytical technique is widely used for identifying and characterizing the molecular composition of materials by measuring the absorption of infrared radiation at different wavelengths. In this study, the FTIR spectra were captured in transmission mode over a scanning range of 4000 to 400 cm^{-1}, which covers the entire infrared region relevant for detecting various functional groups. Each spectrum provides detailed information about the molecular vibrations and chemical bonds present in the sample, allowing for the identification of specific functional groups such as silicates, carbonates, and hydroxyls.

Figure 3.3. FTIR device.

3.3.4. Thermogravimetric Analysis

Thermogravimetric analysis (TGA) was conducted to evaluate the thermal stability and decomposition behaviour of the prepared materials using a Perkin Elmer STA 6000 simultaneous thermal analyzer (Figure 3. 4). This advanced instrument combines the capabilities of thermogravimetric analysis and differential scanning calorimetry, allowing for concurrent measurement of weight changes and heat flow. The analysis was performed under ambient atmospheric conditions, with samples heated from 30°C to 950°C at a relatively rapid heating rate of 10°C per minute (corrected from 100°C/min, which is likely an error). This temperature range was chosen to encompass the typical decomposition temperatures of cement hydration products and other relevant phases.

Figure 3.4. TGA device.

3.4. IN VITRO ANTIBACTERIAL ACTIVITY

The Gentamicin sulphate (Merck-Germany) compound was dissolved in distilled water at a concentration of 2 mg/mL. Subsequently, the resulting aqueous solution was combined with the powder to formulate the cement. The broth microdilution method was used to determine the antimicrobial activity of the samples [86]. Sample extracts were prepared by following ISO 10993 standards for biomaterial testing with a recommended concentration of 0.2 g/mL in sterilized LB broth media. The extracts were incubated for 24 h, at 37°C then sterilized by a 0.22 µm pore-sized filter. The serial dilutions (0.2 g/mL, 0.1 g/mL, 0.05 g/mL, 0.025 g/mL, 0.0125 g/mL, 0.00625 g/mL) were prepared from the extract with an initial 0.2 g/ml concentration in 96 well plates. Staphylococcus aureus (*S. aureus*, gram-positive, ATCC 6538) was cultured overnight at 37°C following the aseptic technique requirements. For the optical density (OD) control, the overnight culture of S. aureus was sub-cultured, and the OD600 values were measured hourly. 10 µl of S. aureus samples (OD600=0.4) were inoculated in 96 well plates with the extracts. The OD600 measurements were repeated at 0 h and 24 h with the microplate reader.

3.5. IN VITRO CELL CULTURE STUDIES

3.5.1. Cell Culture Preparation

The Gentamicin antibiotic was solubilized in distilled water at a concentration of 2 mg/ml. Subsequently, the resulting aqueous solution was combined with the powder to formulate the cement groups. The Osteosarcoma (Saos-2) cell line was cultured in Dulbecco's MEM (DMEM; Merk Germany) containing 10% heat-inactivated fetal bovine serum (FBS) and 1% penicillin/streptomycin (Invitrogen, USA) at 37 °C in a 5% CO_2 containing environment.

3.5.2. Cell Viability Assay

The effect of target samples on the viability of Saos-2 cells was determined using the Deep Blue assay. The compressed and disc-formed versions of the samples were UV sterilized, and discs were placed in a 24 well plate containing DMEM and incubated for 24 h. After the incubation, the media was discarded, and 1×10^4 Saos-2 cells were seeded in a 20 µL drop-on disc sample. After 2 h for the cells to attach to the discs, the medium was completed to 100 µL, and the plate was incubated at 37 °C. For the Deep Blue assay, Deep Blue reagent was added to each well to obtain a 10% final concentration, and the plate was incubated for 4h. After incubation, the Deep Blue reagent-containing media was transferred into the new 24-well plate for fluorescence measurement. Since the deep blue reagent does not harm the cells, after removing the deep blue reagent-containing media, Saos-2 cells continued to grow with adding the fresh medium. A microplate reader (Varioskan Flash Spectral Scanning Multimode Reader, Thermo Scientific) was used for the 530–590 nm fluorescence measurement. The measurements were repeated on day 1, day 4, and day 7.

CHAPTER 4

RESULTS AND DISCUSSION

4.1. MICROSTRUCTURE ANALYSIS OF β-DICALCIUM SILICATE

(Figure 4.1) displays the XRD patterns of β-C_2S powder synthesized using the sol-gel method. These patterns align with the established diffraction data for β-C_2S (PDF#33-0302) [87]. The produced powders had no impurities, like calcium oxide (CaO) and silicon dioxide (SiO_2) [88]. The synthesized C_2S displayed a respectable level of crystallinity, as evidenced by the diffraction peaks that emerged in crisp, narrow forms. The calculated degree of crystallinity was 82.6%.

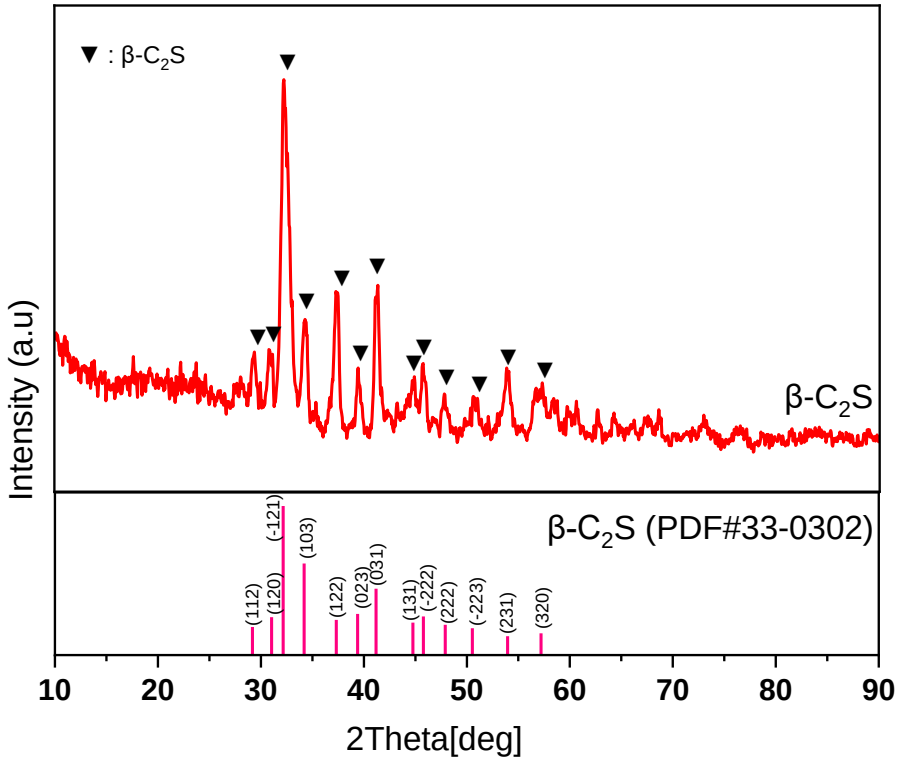

Figure 4.1. XRD pattern of β-C_2S powder calcined at 800◦C for 3 h.

The FTIR spectra of β-C_2S powder are illustrated in (Figure 4.2), with the distinctive peaks of β-C_2S detailed in Table 4.1. The silicate clusters exhibit distinct absorption bands. Notably, prominent peaks at 484 cm^{-1} are associated with the asymmetric bending mode Si-O ν_4 (SiO_4^{-4}). The peak observed at 947 cm^{-1} is also associated with the asymmetric bending mode Si-O ν_3 (SiO_4^{-4}) [89]. Bands within the spectral range of 1216 – 1441 cm^{-1} have also been detected, suggesting a marginal presence of carbon dioxide [90]. Furthermore, a peak at the wavelength of 1740 cm^{-1} nanometers suggests the absorption band is primarily linked to the nitrate ion (NO_3^{-1}) [91]. The band observed at a wavenumber of 3004 cm^{-1} corresponds to the vibrational mode associated with stretching the O-H bonds.

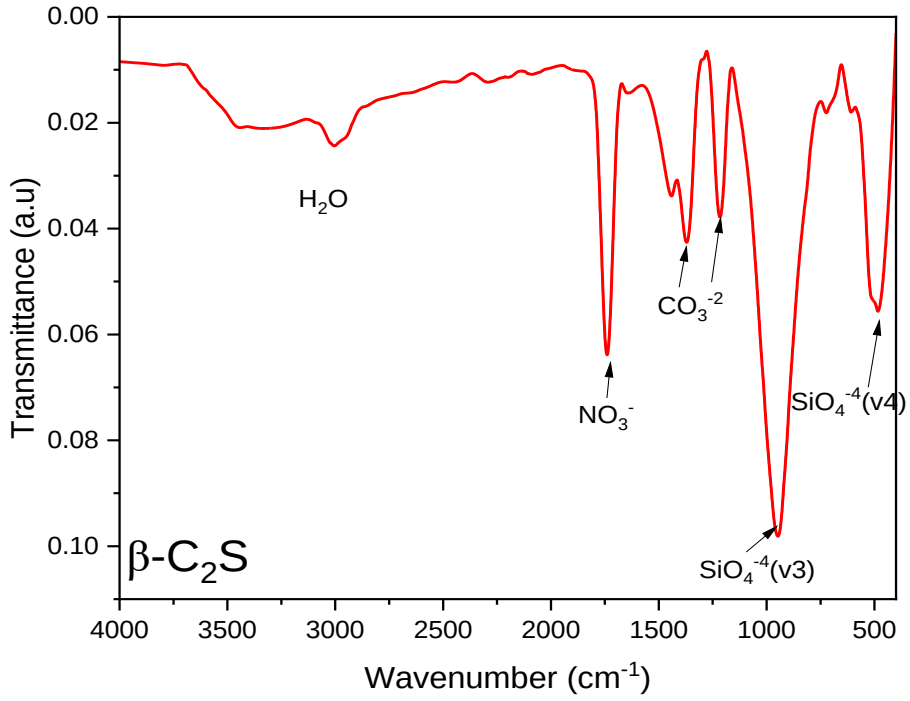

Figure 4.2. FTIR pattern of β-C_2S powder calcined at 800◦C for 3h.

Table 4.1 presents the characteristic peaks observed in the FTIR spectrum of β-C_2S. This table summarizes the key spectral features indicative of the molecular structure and composition of β-C_2S. The data includes six significant peaks, their corresponding wavelengths in wavenumbers (cm^{-1}), and the associated band assignments. These assignments provide information about the molecular vibrations and bonds in the β-C_2S structure, including Si-O bending modes, C-O stretching, the presence of nitrate

ions, and O-H bond stretching. This spectral information is crucial for identifying and characterizing β-C_2S in various applications, particularly cement chemistry and materials science.

Table 4.1. Characteristic peaks of β-C_2S in the FTIR spectrum.

Peak number	**Wavelength (cm^{-1})**	**Band assignment**
1	484	the asymmetric bending mode Si-O ν_4 (SiO_4^{-4})
2	947	the asymmetric bending mode Si-O ν_3 (SiO_4^{-4})
3	1216	stretching C-O
4	1441	stretching C-O
5	1740	the nitrate ion (NO_3^{-1})
6	3004	the stretching of the O-H bonds

The SEM image of β-C_2S powder reveals a detailed view of its microstructure (Figure 4.3). The image shows a rough and irregular surface morphology with a cohesive and interconnected texture. The particles appear to be closely packed and interlocked, which can enhance the mechanical stability of the material when used as a cement precursor. Small pores are visible throughout the structure, contributing to the overall porosity of the material. These pores can influence the material's reactivity and hydration properties. The particles exhibit a relatively uniform size, with an average particle size of approximately 16.6 μm [92]. The image was taken at a magnification of 10,000x, with a scale bar indicating 10 μm for reference, allowing for detailed observation of the microstructural features. This microstructure is typical of β-C_2S and is crucial in its properties and performance in cement applications.

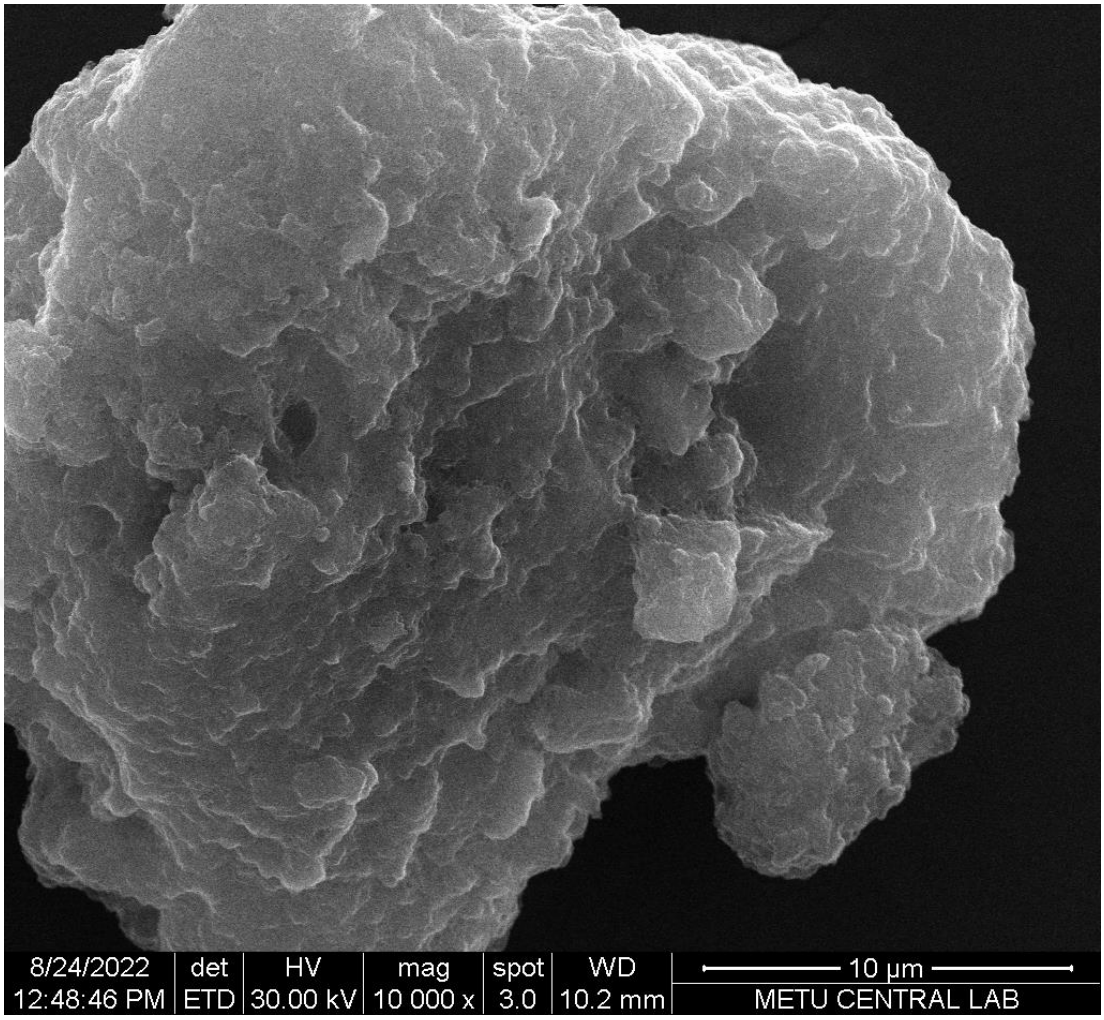

Figure 4.3. SEM image of β-C_2S powder calcined at 800◦C for 3h.

4.2. MICROSTRUCTURE ANALYSIS OF B-TCP

The XRD pattern of β-TCP powder is illustrated in (Figure 4.4), exhibiting a diffraction pattern indicative of the β-TCP phase. The detected peaks strongly correlated with the standard β-TCP reference pattern, specifically the whitlockite phase (JCPDS 09-0169). Notably, the analysis revealed no additional calcium phosphate (CaP) phases. The absence of a distinctive peak at 32.196° confirmed the homogeneity of the synthesized powder and the successful exclusion of the hydroxyapatite (HA) phase (JCPDS 09-432). This outcome is consistent with previous research findings, lending further credence to the reliability and reproducibility of the β-TCP synthesis methodology employed in this study [93]. Basically, the XRD results show that the synthesis of β-TCP was successful and pure, with no other calcium phosphate phases

getting in the way. This purity is crucial for ensuring the material's intended properties and performance in subsequent applications.

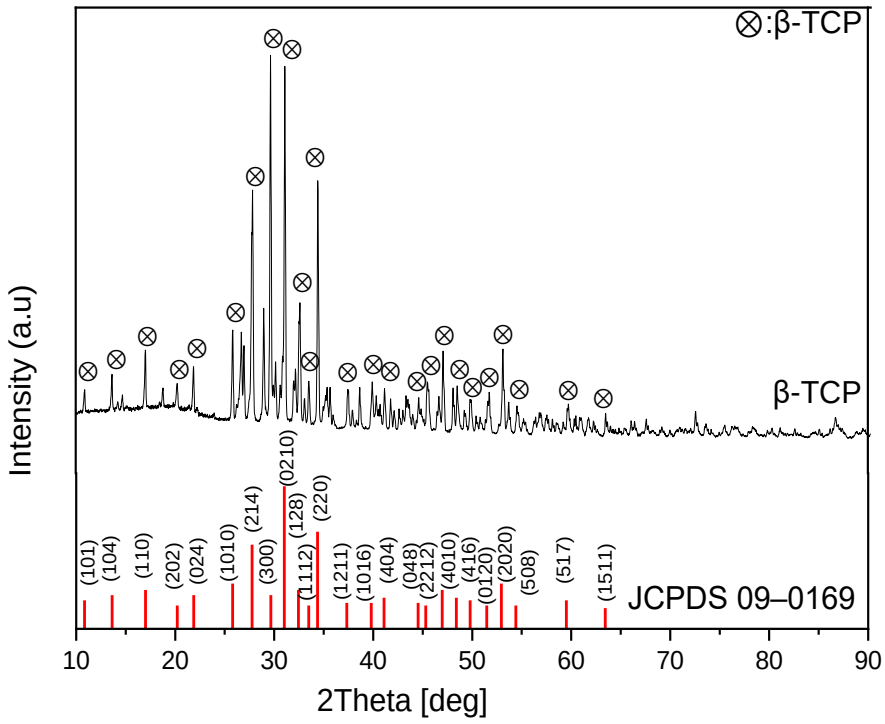

Figure 4.4. XRD pattern of β-TCP calcined at 1000 ºC for 2 h.

The SEM images revealed the spherical shape and smooth surface of the β-TCP powder (Figure 4.5). These observations suggest particle fusion, likely due to the high-temperature heat treatment employed. This is consistent with previous reports, where microwave-assisted synthesis followed by calcination at 1000 °C for 2 hours resulted in β-TCP particles with an average size of ~150 nm [94–96]. The observed particle size in our study is larger than reported in some prior studies, potentially due to accelerated particle growth during the high-temperature treatment. Furthermore, the Ca/P ratio 1.39 was slightly lower than the stoichiometric value of 1.5 for β-TCP. This deviation from the ideal stoichiometric ratio may indicate the presence of calcium-deficient β-TCP or trace amounts of other calcium phosphate phases not detectable by XRD. The lower Ca/P ratio could potentially affect the material's properties, such as solubility and bioactivity, and warrants further investigation to understand its implications on the material's performance in biomedical applications.

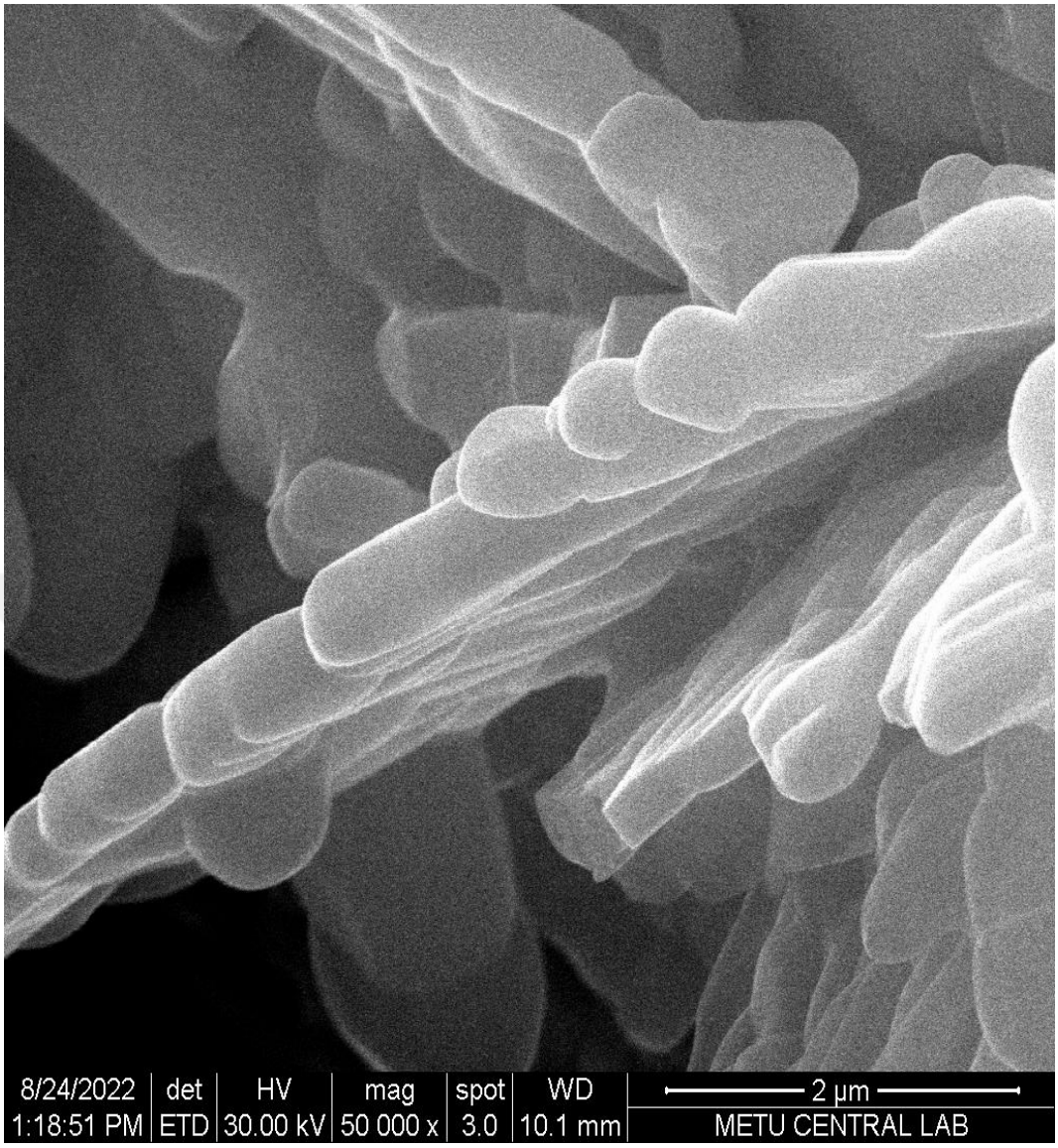

Figure 4.5. SEM image of β-TCP sample calcined at 1000 ºC for 2 h.

The FTIR spectra of the β-TCP- powders are presented in (Figure 4.6). (Table 4.2) details the characteristic peaks associated with β-TCP observed in the FTIR spectrum. The band at 551.07 cm^{-1} corresponds to the ν_4 vibrational mode of the PO_4^{3-} ion, consistent with previous studies [97,98]. These peaks' positions and morphologies closely resemble those described in the literature [99]. Notably, a peak at 724 cm^{-1} suggests the presence of residual $P_2O_7^{-4}$ ions, potentially originating from the β-calcium pyrophosphate (β-$Ca_2P_2O_7$) precursor used during the synthesis of β-TCP. The increased sharpness of the peak observed in the FTIR spectrum corroborates the

transformation of HPO_4^{-2} into β-TCP upon calcination at 1000°C. This transformation is further supported by bands assigned to the ν_1 (symmetric stretching) and ν_3 (asymmetric stretching) modes of the PO_4^{-3} group within the wavenumber range of 937.97 cm^{-1} to 1214.32 cm^{-1}. These peak positions and morphologies closely resemble those reported in previous FTIR analysis studies [98,100]. The bands identified at 1022.72 cm^{-1} and 1066.93 cm^{-1} can be attributed to the characteristic stretching vibrations associated with ν_3 mode [101]. Furthermore, the peak at 1144.31 cm^{-1} likely corresponds to the triply degenerate ν_3 antisymmetric P-O stretching modes [102]. The presence of a signal at 1365.4 cm^{-1} suggests the existence of residual nitrate groups, potentially originating from the synthesis precursors [103]. The absorption band observed at 1733 cm^{-1} can be ascribed to the characteristic peak associated with the C=O bond [104]. Notably, the absence of stretching and bending bands around 3001 cm^{-1}, which are typically attributed to the hydroxyl (-OH) group, validates the successful synthesis of a single-phase β-TCP [98].

Table 4.2. Characteristic peaks of β-TCP in the FTIR spectrum.

Peak number	**Wavelength (cm^{-1})**	**Band assignment**
1	551.07	$PO4^{-3}$ vibrational mode of (υ4)
2	724	$P_2O_7^{-4}$ ions
3	937.97	$PO4^{-3}$ symmetric stretching mode of (υ1)
4	1022.72	$PO4^{-3}$ asymmetric stretching mode of (υ3)
5	1066.93	$PO4^{-3}$ asymmetric stretching mode of (υ3)
6	1144.31	$PO4^{-3}$ asymmetric stretching mode of (υ3)
7	1214.32	$PO4^{-3}$ asymmetric stretching mode of (υ3)
8	1365.4	the nitrate ion (NO^{-3})
9	1733	the C=O bond
10	3001	the stretching of the O-H bonds

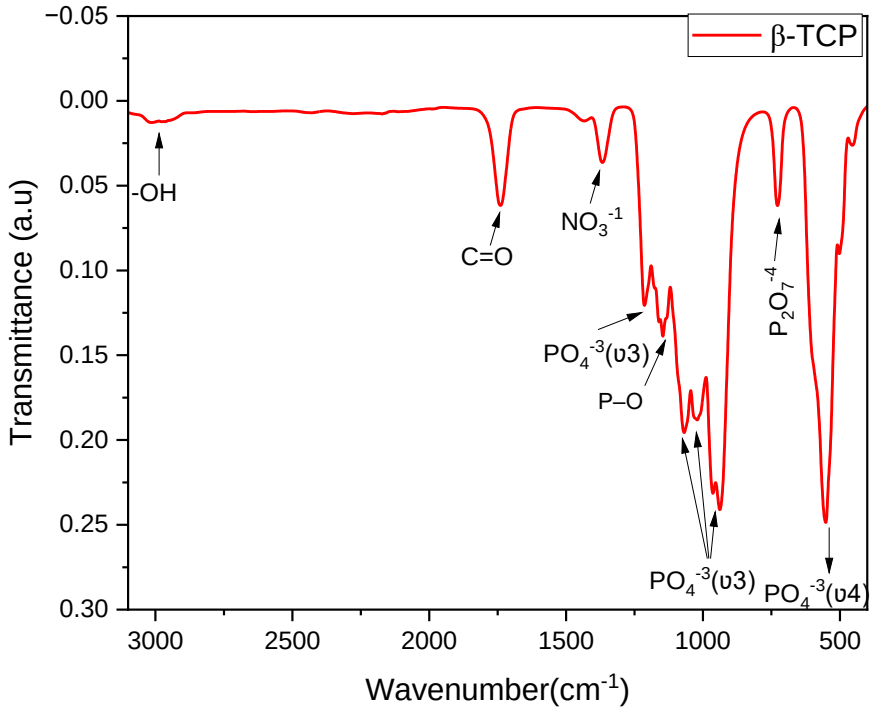

Figure 4.6. FTIR spectrum of β-TCP powder that underwent calcination at 1000 °C for 2 hrs.

4.3. MICROSTRUCTURE AND BIOLOGICAL PROPERTIES OF DICALCIUM PHOSPHATE/CALCIUM SILICATE HYDRATE CEMENT COMPOSITES

(Figure 4.7) depicts the XRD patterns of cement samples prepared in accordance with the guidelines outlined in (Table 3.1). The specimens were subjected to a 24-hour preparation period in a water bath maintained at 37 °C and a relative humidity of 100% [105]. The data is presented in (Figure 4.7) illustrates the occurrence of peaks at 2θ = 29.356°, 32.054°, and 50.079°, indicating the presence of CSH. This compound is formed due to the hydration of β-C_2S and exhibits a relatively low degree of crystallinity [50]. This observation is consistent with established diffraction data about CSH, as documented in (PDF#33-0306). (Figure 4.7) depicts cement's XRD pattern with a 20% incorporation of DCP. A discernible reduction in the maximum intensity was observed at an angle of 2 = 29.356° after incorporating DCP into the cement

mixture. The observed alterations in the XRD pattern indicate a decrease in particle dimensions and a decrease in the degree of crystallinity within the particles (Table 4.2.). The enhanced interaction between the larger DCP molecules and the crystal lattice led to an expansion of the dimensions of the unit cell. This broadening is believed to be the reason for the observed shift of the diffraction peak towards lower angles. Increasing to 30% DCP resulted in a more significant decrease in the lattice parameters, which we can see from the table, where the value of Å = 5.50343 (a) decreased as well as an overall decrease in the crystallinity level of 95.710% [73,106].

Table 4.3. Lattice parameters, cell size, and degree of crystallinity of the samples.

Sample ID	**Å (A)**	**C(Å)**	**CV(Å)^3**	**Crystallinity (٪)**	**Crystallite size (nm)**
JCDPS (β-C_2S)	9.3100	5.5059	345.29	-------	-------
CSH	8.68271	6.39536	420.5514	92.66 %	19.8 nm
20 % DCP/ CSH	5.50574	6.75457	345.3645	98.763 %	21.1 nm
30 % DCP/ CSH	5.50343	6.76635	346.2943	95.710 %	21.4 nm
40 % DCP/ CSH	5.30777	6.75693	345.3189	91.6 %	22 nm

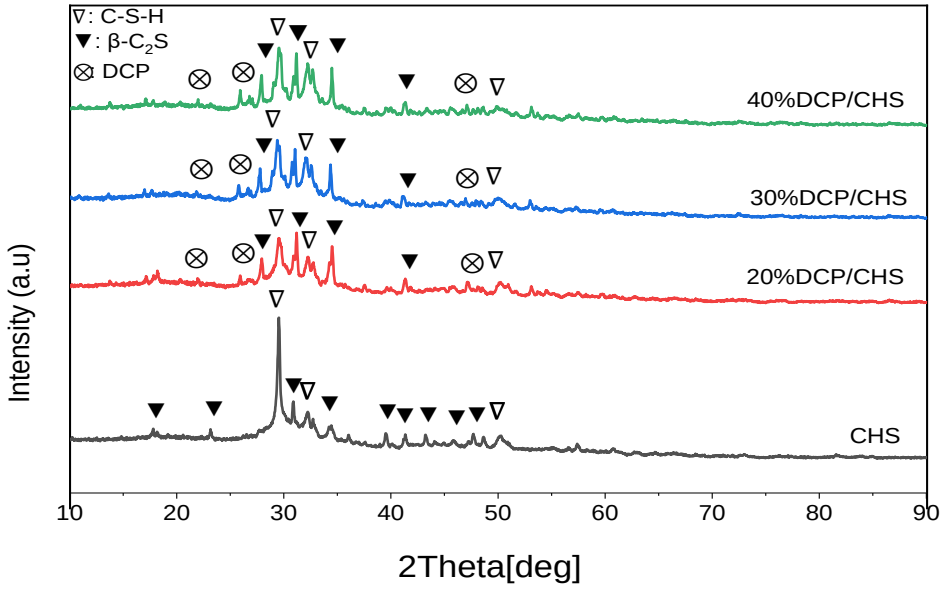

Figure 4.7. XRD pattern of pure CSH and DCP/CSH composite cement.

(Figure 4.8) presents the FTIR spectra of the cement samples produced per the specifications outlined in (Table 3.1) The samples were subjected to a 24-hour preparation period in a water bath maintained at a temperature of 37 °C and a relative humidity of 100%. Distinct absorption bands associated with the silicate clusters can be observed in (Figure 4.8). It is important to acknowledge that there exist prominent peaks at 460 cm^{-1}, which can be associated with the asymmetric bending mode Si-O v4 (SiO_4^{-4}), while the peak at 946 cm^{-1} is attributed to the asymmetric bending mode Si-O $v_3(SiO_4^{-4})$ [107]. Bands within the spectral range of 1217 – 1426 cm^{-1} have also been detected, suggesting a marginal presence of carbon dioxide [105]. The spectral peak observed at approximately 1642 cm^{-1} is attributed to the asymmetric stretching of the H-O-H bending vibrations within the H_2O molecule.

Furthermore, a peak at 1738 cm^{-1} signifies the absorption band primarily linked to NO_3^{-1} [91]. The spectral region approximately centred at 3336 cm^{-1} is attributed to the vibrational modes of hydroxyl groups in H_2O undergoing stretching motions, which exhibit a range of hydrogen bond strengths [90]. The subsequent bands were observed upon adding 20% DCP to the cement. The spectral peaks observed at 558 and 535 cm^{-}

[1] are assigned to the stretching vibration of the P-O-H group in HPO_4^{-2}, while the peak at 1376 cm^{-1} is attributed to the stretching vibration of the P-O-H group in HPO_4^{-2}, which is in agreement with the formation of dicalcium phosphate (DCP). When the DCP ratio is increased from 30% to 40%, a marginal rise is observed in the characteristic peaks at 889 and 995 cm^{-1}, which can be attributed to the P-O stretching mode of HPO_4^{-2} [108].

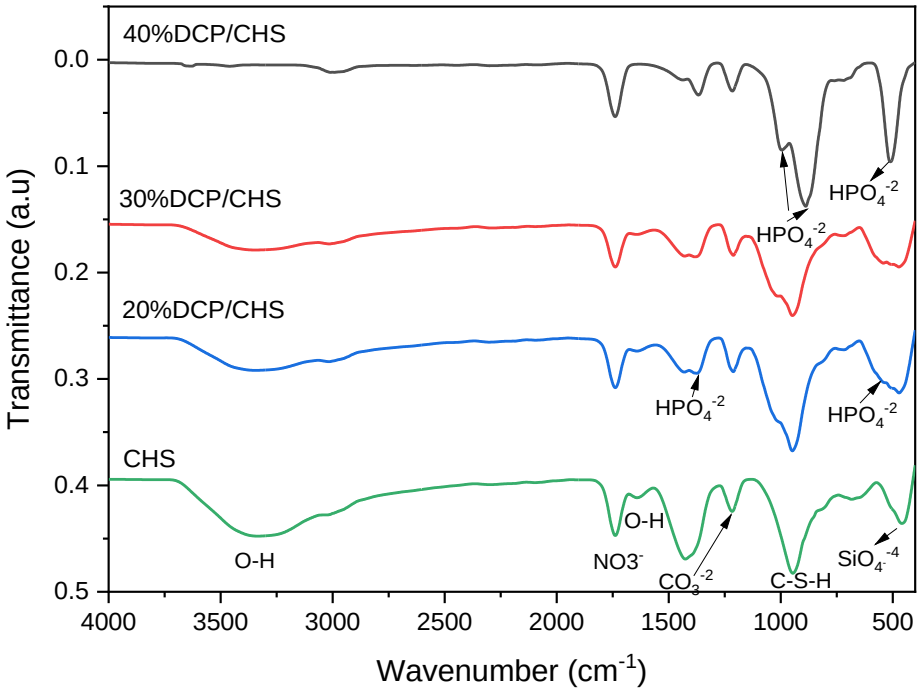

Figure 4.8. FT-IR pattern of pure CSH and DCP/CSH composite cement.

Table 4.4. Characteristic peaks pure CSH cement and DCP/ CSH composite cement.

Peak number	**Wavelength (cm^{-1})**	**Band assignment**
1	460	the asymmetric bending mode Si-O v4 (SiO_4^{-4})
2	946	the asymmetric bending mode Si-O v3 (SiO_4^{-4})
3	1214	stretching C-O
4	1426	stretching C-O
5	1783	the nitrate ion (NO_3^{-1})
6	3336	the stretching of the O-H bonds
7	535	Stretching vibration of P-O-H group in HPO_4^{-2}
8	558	Stretching vibration of P-O-H group in HPO_4^{-2}
9	1376	Stretching vibration of P-O-H group in HPO_4^{-2}

(Figure 4.9) depicts the microstructure of pure CSH cement and DCP/CSH composite cement. The cement had a very complex structure, which was shown by the formation of small pores and a fibrous surface on the cement particles. The addition of 20% DCP results in the formation of flake-like particles on the cement surface and a reduction in pore size. When the DCP ratio is increased to 40%, the presence of flake-like particles becomes more evident [109,110].

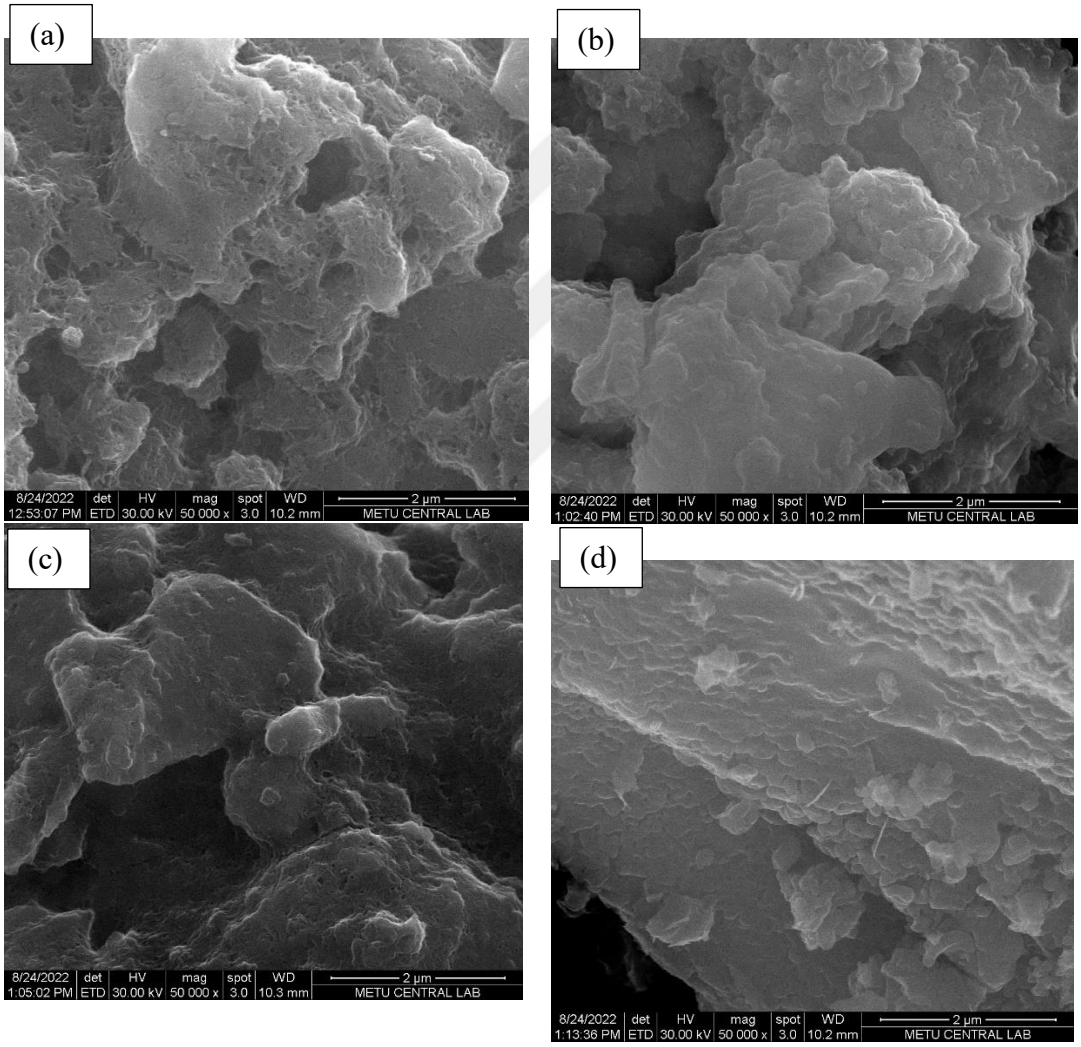

Figure 4.9. SEM images of (a) pure CHS, (b) 20%DCP/CSH, (c) 30%DCP/CSH, and (d) 40%DCP/CSH composite cement.

(Figure 4.10) presents the thermal analysis results, specifically the TGA/DTA, for the cement samples produced by the specifications outlined in Table 3.1. The pure CSH cement exhibits three distinct weight loss stages at temperatures of 30-300°C, 300-600°C, and 600-700°C. The initial phase of the process, occurring within a temperature range of 30-300 °C, primarily focuses on eliminating any remaining moisture and chemically bonded water. It is worth noting that there may also be traces of residual ethanol present during this stage [73]. The decomposition of the nitrate compound employed in the solution formulation seems to align with the second phase, which occurs within 300–600 °C [107]. The third stage, which occurs at temperatures ranging from 600 to 700 °C, is characterized by the decomposition of organic substances and the degradation of $CaOH_2$. We observe no significant weight reduction at temperatures exceeding 700°C. This observation was further confirmed at 800 °C, suggesting that the samples attain a state of stability following calcination at temperatures surpassing the threshold [89]. The incorporation of DCP into the cement mixture resulted in a decrease in the rate of weight loss. Furthermore, all sample specimens demonstrated the ability to withstand temperatures of 700 °C or higher. The respective weight loss percentages for pure CSH, 20% DCP/CSH, 30% DCP/CSH, and 40% DCP/CSH were 26.048%, 20.631%, 16.662%, and 10.539%.

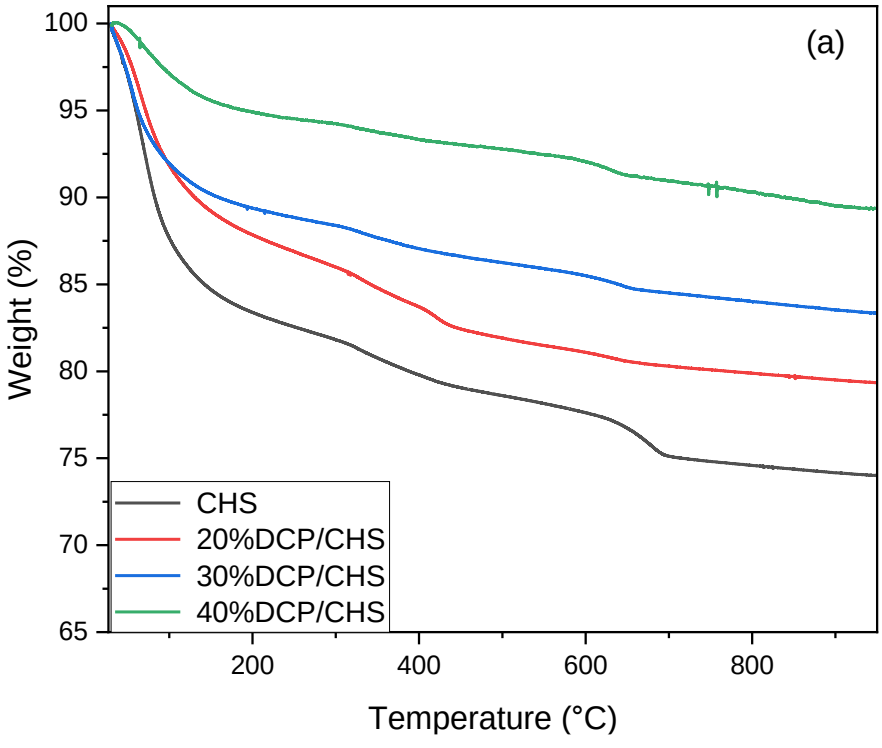

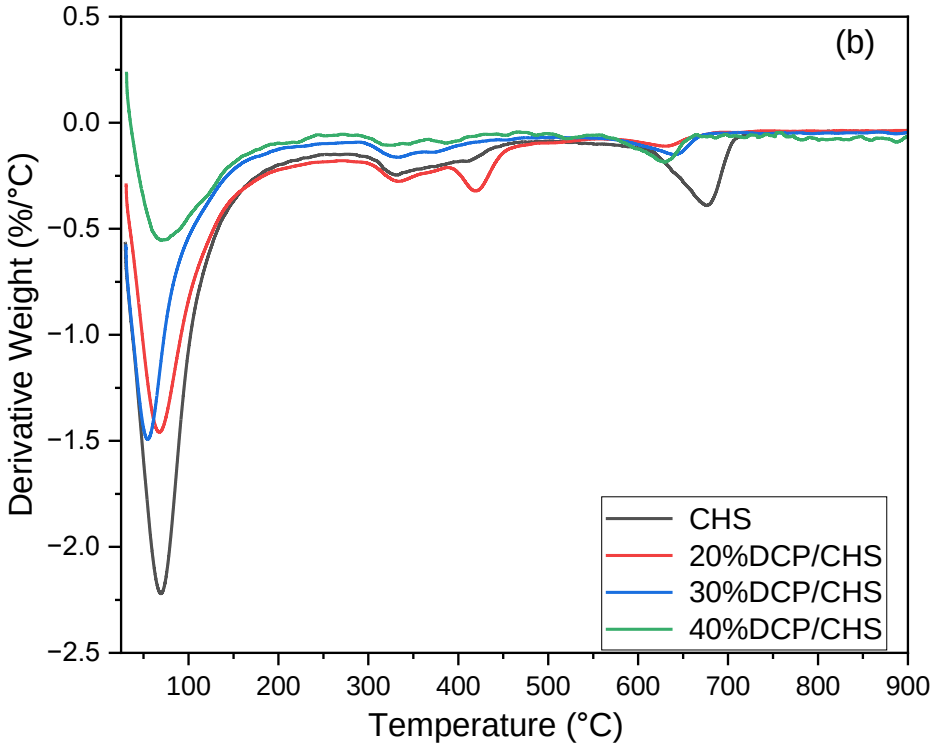

Figure 4.10. Thermograms of pure CHS and DCP/CHS composite cement: (a) TGA, (b) DTA

Using OD600 measurements, the quantity of S. aureus bacteria in the presence or absence of extracts of cement samples loaded with gentamicin antibiotic was assessed, demonstrating the antibacterial efficacy of hybrid cement. The test samples in this study exhibited antimicrobial activity at various concentrations, aligning with previous studies. Calcium silicate-based cements are believed to exhibit antimicrobial activity due to their high alkalinity [111].

Notably, the pure CSH cement loaded with gentamicin exhibited the most potent antibacterial efficacy at a concentration of 0.2 g/mL. However, incorporating DCP loaded with gentamicin at a rate of 20% mitigated this effect. The observed antibacterial activity continued to decline as the DCP concentration increased to 40%, ultimately facilitating bacterial proliferation.

According to the data presented in (Figure 4.11) both the 20% DCP/CSH cement and the 40% DCP/CSH cement demonstrated the highest level of antibacterial activity at a

concentration of 0.05 g/mL. At a 0.00625 g/mL concentration, none of the cement types displayed antibacterial properties. However, at higher concentrations, all groups showed antibacterial activity.

The cement extracts were prepared by incubating cement discs with LB broth, during which gentamicin loaded into the cements was expected to be released. The results showed that gentamicin-loaded cement at concentrations of 0.00625 g/mL and higher was able to release sufficient gentamicin to create antibacterial activity after 1 day of incubation.

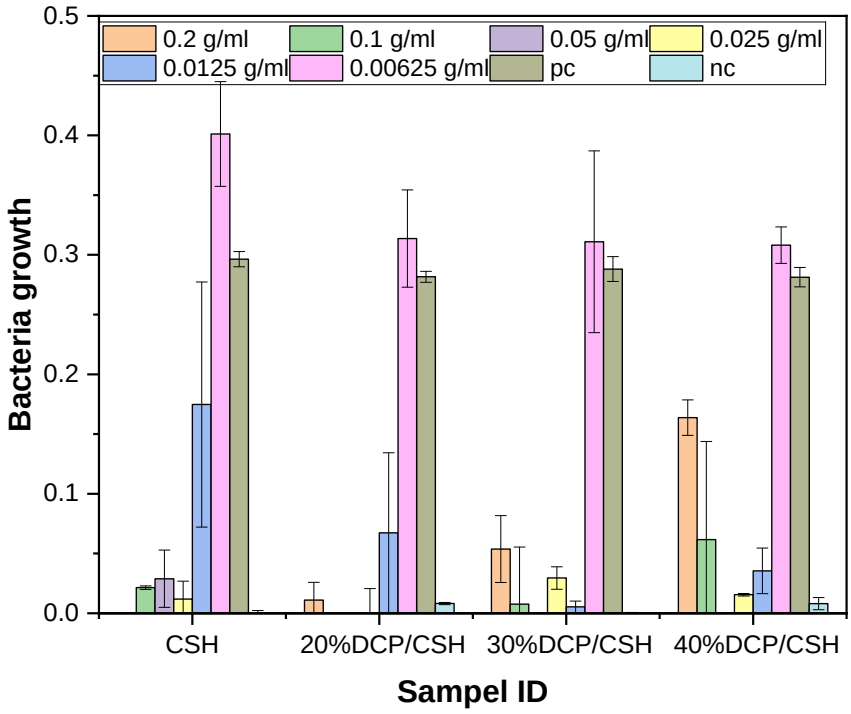

Figure 4.11. Effect of pure CSH and DCP/CSH composite cements on *S. aureus*.

(Figure 4.12) (a, b) displays the results of cell viability analysis when Saos-2 cells were subjected to cement groups loaded with gentamicin. The Deep Blue assay results show that Saos-2 cell viability has decreased on pure CSH cement compared to cell viability on well plates (Figure 4.12 (a)). Cell viability on pure CSH cement through 1, 4, and 7 days was roughly 18.76%, 34.68%, and 46.84%, respectively. When the cement group was prepared with the addition of 20% DCP, cell viability improved to 21.04%,

58.14%, and 73.74% through 1, 4, and 7 days of incubation. The observed effects declined as the concentration of DCP was elevated to between 30% and 40%. CSH is known to create a favourable environment for the life cycle of Saos-2 cells [112]. In addition, calcium is one of the leading players in the intracellular signalling pathways [113,114]. It has also been reported that an excess of intracellular calcium can lead to a wide range of deleterious effects for cells [115]. When the results obtained in this study are evaluated from this perspective, it can be speculated that the positive effect of 20% DCP on cellular growth and the negative effect of increasing DCP levels on growth are consistent with the role of Ca in the cell.

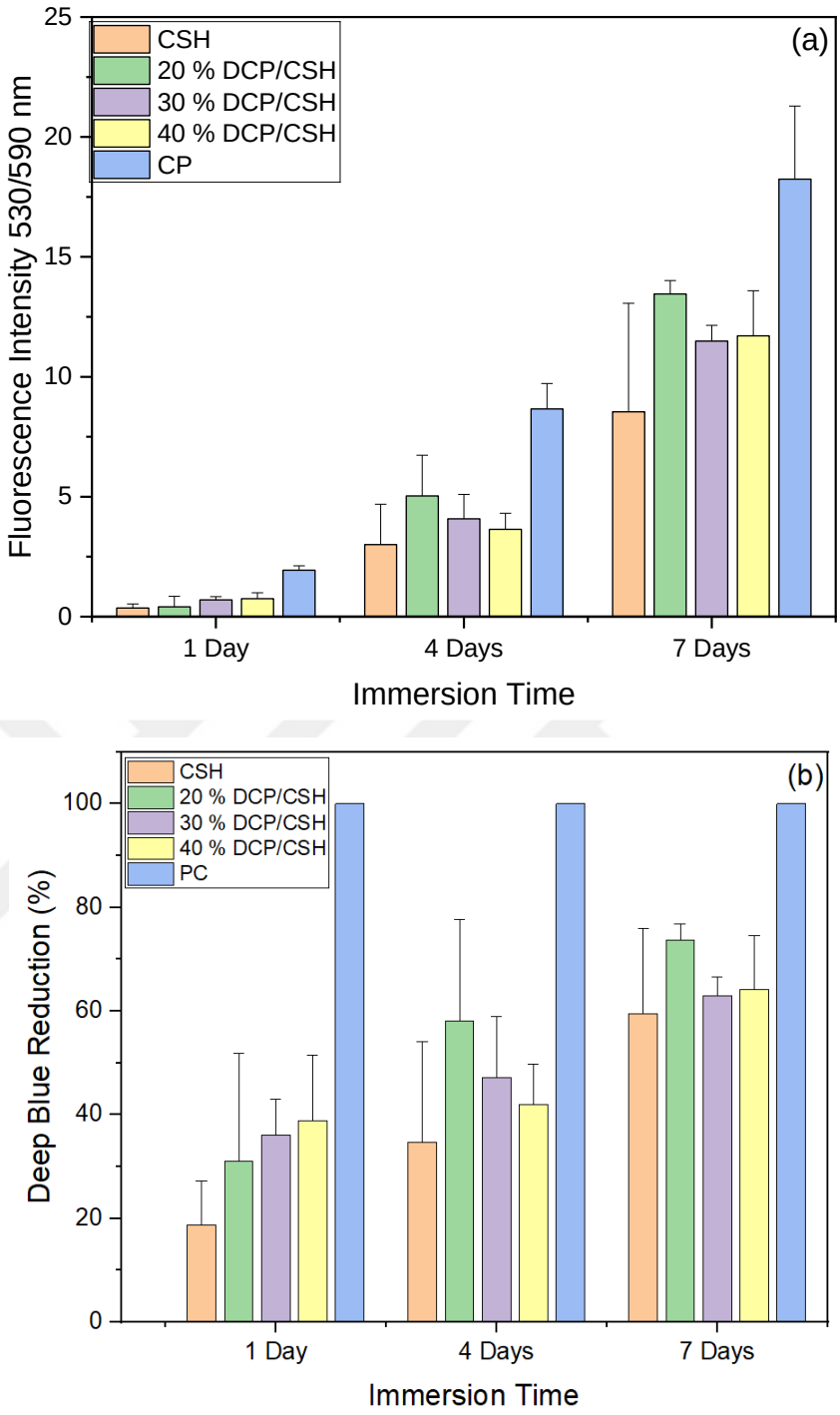

Figure 4.12. Effect of pure CHS and DCP/CHS composite cement on the proliferation of Saos-2 cells as measured by Deep Blue Cell Viability Assay. (a) Fluorescence intensity at 530/590 nm, (b) Reduction ratio, over a 7-day period.

CHAPTER 5

CONCLUSION

The research successfully synthesized β-Dicalcium Silicate (β-C_2S) using the sol-gel method and utilized it as a precursor to prepare calcium silicate hydrate (CSH) cement. The study investigated the effects of incorporating different dicalcium phosphate (DCP) fractions into CSH cement on its microstructural and biological properties. The results demonstrated that adding DCP significantly influences the properties of the cement composites.

The microstructural analysis revealed that incorporating DCP at 20%, 30%, and 40% fractions into CSH cement resulted in crystallinity and particle size changes. Specifically, the X-ray diffraction (XRD) patterns indicated decreased crystallinity and particle size with increasing DCP content. The Fourier Transform Infrared (FTIR) spectroscopy confirmed the presence of characteristic peaks for both CHS and DCP, indicating successful incorporation.

Thermal analysis (TGA/DTA) showed that the cement composites exhibited distinct weight loss stages, with the pure CSH cement losing 26.048% of its weight. In comparison, the 20%, 30%, and 40% DCP/CSH composites lost 20.631%, 16.662%, and 10.539%, respectively. These results suggest that adding DCP enhances the cement composites' thermal stability.

The antibacterial tests demonstrated that the CHS cement loaded with gentamicin exhibited the highest antibacterial efficacy at 200 mg/ml concentration. However, the antibacterial activity decreased with the addition of DCP, with the 20% DCP/CSH composite showing the highest antibacterial activity at a concentration of 50 mg/ml. The biocompatibility tests using Saos-2 cells indicated that the pure CSH cement

significantly reduced cell viability, while the addition of DCP improved cell viability, with the 20% DCP/CSH composite showing the most substantial improvement.

RECOMMENDATIONS FOR FUTURE WORKS

To build upon the findings of this research, the following recommendations are proposed for future studies:

- Future research should focus on optimizing the composition of the cement by exploring different ratios of DCP and other additives to enhance the mechanical properties and setting time. The inclusion of cohesiveness boosters such as chitosan, gelatin, and cellulose could be investigated to improve the cement's performance.
- Comprehensive in vivo studies are necessary to evaluate the long-term biocompatibility, mechanical stability, and degradation behavior of the cement composites. These studies should include animal models to simulate the physiological conditions and assess the cement's performance over extended periods.
- Employing advanced characterization techniques such as nanoindentation and micro-computed tomography (micro-CT) can provide deeper insights into the microstructural properties and mechanical behavior of cement composites. These techniques can help understand the material's interaction with bone tissue at the nanoscale level.
- Investigating the effects of incorporating other bioactive materials, such as hydroxyapatite, bioactive glass, and magnesium phosphate, could further enhance the cement's osteoconductivity and bioactivity. These materials may provide additional benefits in promoting bone regeneration and integration.
- Research should explore the development of injectable cement formulations that can be easily administered in minimally invasive procedures. This approach can improve the ease of application and reduce the need for extensive surgical interventions.

By addressing these recommendations, future research can further enhance the potential of DCP/CSH cement composites as effective materials for bone regeneration and repair, ultimately contributing to advancements in orthopedic and dental treatments.

REFERENCES

1. Olszta, M. J., Cheng, X., Jee, S. S., Kumar, R., Kim, Y. Y., Kaufman, M. J., Douglas, E. P., and Gower, L. B., "Bone structure and formation: A new perspective", ***Materials Science And Engineering: R: Reports***, 58 (3–5): 77–116 (2007).

2. Rho, J.-Y., Kuhn-Spearing, L., and Zioupos, P., "Mechanical properties and the hierarchical structure of bone", 20.2: 92-102 (1998).

3. Ralston, S. H. Bone structure and metabolism. *Medicine*, *41*(10): 581-585 (2013).

4. Liu, Yan, Dan Luo, and Tie Wang. "Hierarchical structures of bone and bioinspired bone tissue engineering." *Small* 12.34: 4611-4632 (2016).

5. Imbert, L., Gourion-Arsiquaud, S., Villarreal-Ramirez, E., Spevak, L., Taleb, H., van der Meulen, M. C. H., Mendelsohn, R., and Boskey, A. L., "Dynamic structure and composition of bone investigated by nanoscale infrared spectroscopy", ***PLOS ONE***, 13 (9): 1-15 (2018).
6. Schemitsch, E. H., "Size Matters: Defining Critical in Bone Defect Size!", ***Journal Of Orthopaedic Trauma***, 31: 20-22 (2017).

7. Hsiong, Susan X., and David J. Mooney. "Regeneration of vascularized bone." *Periodontology 2000* 41.1: 109-122 (2006).

8. Sadeghzade, S., Liu, J., Wang, H., Li, X., Cao, J., Cao, H., Tang, B., and Yuan, H. Recent advances on bioactive baghdadite ceramic for bone tissue engineering applications: 20 years of research and innovation (a review). ***Materials Today Bio*****,** *17*, 100473: 1-27 (2022).

9. Wei, Y., Zhu, G., Zhao, Z., Yin, C., Zhao, Q., Xu, H., Wang, J., Zhang, J., Zhang, X., Zhang, Y., and Xia, H., "Individualized plasticity autograft mimic with efficient bioactivity inducing osteogenesis", ***International Journal Of Oral Science***, 13 (1): 1-8 (2021).

10. Srinath, P., Abdul Azeem, P., and Venugopal Reddy, K., "Review on calcium silicate-based bioceramics in bone tissue engineering", ***International Journal Of Applied Ceramic Technology***, 17 (5): 2450–2464 (2020).

11. Zhang, J., Liu, W., Schnitzler, V., Tancret, F., and Bouler, J. M.. Calcium phosphate cements for bone substitution: chemistry, handling and mechanical properties. ***Acta biomaterialia***, *10*(3): 1035-1049 (2014).

12. Bakhtiari, S. S. E., Bakhsheshi-Rad, H. R., Karbasi, S., Tavakoli, M., Tabrizi, S. A. H., Ismail, Seifalian, A, RamaKrishna, S, Berto, F. Poly (methylmethacrylate) bone cement, its rise, growth, downfall and future. Polymer International, 9(70): 1182-1201 (2021).

13. Zhou, Huan, Joseph G. Lawrence, and Sarit B. Bhaduri. "Fabrication aspects of PLA-CaP/PLGA-CaP composites for orthopedic applications: a review." *Acta biomaterialia* 8.6: 1999-2016 (2012).

14. Moseke, Claus, and U. Gbureck. "Tetracalcium phosphate: Synthesis, properties and biomedical applications." *Acta Biomaterialia* 6.10: 3815-3823 (2010).

15. Chopra, V., Thomas, J., Kaushik, S., Rajput, S., Guha, R., Mondal, B., Naskar, S., Mandal, D., Chauhan, G., Chattopadhyay, N., and Ghosh, D., "Injectable Bone Cement Reinforced with Gold Nanodots Decorated rGO-Hydroxyapatite Nanocomposites, Augment Bone Regeneration", ***Small***, 19 (14): 1-19 (2023).

16. Pahlevanzadeh, F., Bakhsheshi-Rad, H. R., and Hamzah, E., "In-vitro biocompatibility, bioactivity, and mechanical strength of PMMA-PCL polymer containing fluorapatite and graphene oxide bone cements", ***Journal Of The Mechanical Behavior Of Biomedical Materials***, 82: 257–267 (2018).

17. Ghasemi, F., Jahani, A., Moradi, A., Ebrahimzadeh, M. H., and Jirofti, N., "Different Modification Methods of Poly Methyl Methacrylate (PMMA) Bone Cement for Orthopedic Surgery Applications", ***Archives Of Bone And Joint Surgery***, 11 (8): 485–492 (2023).

18. Shridhar, P., Chen, Y., Khalil, R., Plakseychuk, A., Cho, S. K., Tillman, B, Kumta, P, N, Chun, Y. A review of PMMA bone cement and intra-cardiac embolism. ***Materials***, *9*(10): 1-14 (2016).

19. Saruta, J., Ozawa, R., Hamajima, K., Saita, M., Sato, N., Ishijima, M., Kitajima, H., and Ogawa, T., "Prolonged post-polymerization biocompatibility of polymethylmethacrylate-tri-n-butylborane (Pmma-tbb) bone cement", ***Materials***, 14 (5): 1–16 (2021).

20. Hernández, M. L., Alonso, L. M., Pradas, M. M., Lozano, O. E. L., and Bello, D. G., "Composites of poly(methyl methacrylate) with hybrid fillers (micro/nanohydroxyapatite): Mechanical, setting properties, bioactivity and cytotoxicity in vitro", ***Polymer Composites***, 34 (11): 1927–1937 (2013).

21. Tham, D. Q., Huynh, M. D., Linh, N. T. D., Van, D. T. C., Van Cong, D., Dung, N. T. K., Trang, N. T. T., Van Lam, P., Hoang, T., and Lam, T. D., "Pmma bone cements modified with silane-treated and pmma-grafted hydroxyapatite nanocrystals: Preparation and characterization", ***Polymers***, 13 (22): 1-22 (2021).

22. Correa, D., Almirall, A., García-Carrodeguas, R., Alberto Dos Santos, L., De Aza, A. H., Parra, J., and Ángel Delgado, J., "β-Dicalcium silicate-based cement: Synthesis, characterization and in vitro bioactivity and biocompatibility studies",

Journal Of Biomedical Materials Research - Part A, 102 (10): 3693–3703 (2014).

23. Wang, D., Zhang, Y., and Hong, Z., "Novel fast-setting chitosan/β-dicalcium silicate bone cements with high compressive strength and bioactivity", ***Ceramics International***, 40 (7 PART A): 9799–9808 (2014).

24. Liu, W., Huan, Z., Xing, M., Tian, T., Xia, W., Wu, C., Zhou, Z., and Chang, J., "Strontium-substituted dicalcium silicate bone cements with enhanced osteogenesis potential for orthopaedic applications", ***Materials***, 12 (14): 1-16 (2019).

25. Motameni, A., Alshemary, A. Z., Dalgic, A. D., Keskin, D., and Evis, Z., "Graphene oxide reinforced doped dicalcium phosphate bone cements for bone tissue regenerations", ***Journal Of The Australian Ceramic Society***, 58 (5): 1633–1647 (2022).

26. Motameni, A., Alshemary, A. Z., Dalgic, A. D., Keskin, D., and Evis, Z., "Lanthanum doped dicalcium phosphate bone cements for potential use as filler for bone defects", ***Materials Today Communications***, 26: 1-10 (2021).

27. Tariq, U., Hussain, R., Tufail, K., Haider, Z., Tariq, R., and Ali, J., "Injectable dicalcium phosphate bone cement prepared from biphasic calcium phosphate extracted from lamb bone", ***Materials Science And Engineering C***, 103: 1-9 (2019).

28. Xie, L., Luo, D., Zhu, Y., Xu, C., and Li, Y., "Luminescence and mineralization properties of Gd^{3+} stabilized β-dicalcium silicate", ***Physica B: Condensed Matter***, 610: 1-9 (2021).

29. IEEE Computer Society., IEEE Engineering in Medicine and Biology Society., Sichuan da xue., and Wuhan da xue., "2010 4th International Conference on Bioinformatics and Biomedical Engineering (ICBBE) : June 18-20, 2010 Chengdu, China", ***[IEEE]***, (2010).
30. Huan, Z., Chang, J., and Huang, X. H., "Self-setting properties and in vitro bioactivity of $Ca_2SiO_4/CaSO_4 \cdot 1/2H_2O$ composite bone cement", ***Journal Of Biomedical Materials Research - Part B Applied Biomaterials***, 87 (2): 387–394 (2008).

31. Li, H. and Chang, J., "Stimulation of proangiogenesis by calcium silicate bioactive ceramic", ***Acta Biomaterialia***, 9 (2): 5379–5389 (2013).

32. Li, H. and Chang, J., "Fabrication and characterization of bioactive wollastonite/PHBV composite scaffolds", ***Biomaterials***, 25 (24): 5473–5480 (2004).

33. Li, H., Xue, K., Kong, N., Liu, K., and Chang, J., "Silicate bioceramics enhanced vascularization and osteogenesis through stimulating interactions between

endothelia cells and bone marrow stromal cells", ***Biomaterials***, 35 (12): 3803–3818 (2014).

34. Wang, C., Lin, K., Chang, J., and Sun, J., "Osteogenesis and angiogenesis induced by porous β-$CaSiO_3$/PDLGA composite scaffold via activation of AMPK/ERK1/2 and PI3K/Akt pathways", ***Biomaterials***, 34 (1): 64–77 (2013).

35. Hughes, E., Yanni, T., Jamshidi, P., and Grover, L. M., "Inorganic cements for biomedical application: Calcium phosphate, calcium sulphate and calcium silicate", ***Advances In Applied Ceramics***, 114 (2): 65–76 (2015).

36. Cannillo, V., Pierli, F., Sampath, S., and Siligardi, C., "Thermal and physical characterisation of apatite/wollastonite bioactive glass-ceramics", ***Journal Of The European Ceramic Society***, 29 (4): 611–619 (2009).

37. Sanmartin de Almeida, M., Fernandes, G. V. D. O., de Oliveira, A. M., and Granjeiro, J. M. Calcium silicate as a graft material for bone fractures: a systematic review. *Journal of International Medical Research*, *46*(7): 2537-2548 (2018).

38. Gandolfi, M. G., Siboni, F., Botero, T., Bossù, M., Riccitiello, F., and Prati, C., "Calcium silicate and calcium hydroxide materials for pulp capping: Biointeractivity, porosity, solubility and bioactivity of current formulations", ***Journal Of Applied Biomaterials And Functional Materials***, 13 (1): 1–18 (2015).

39. Papynov, E. K., Shichalin, O. O., Apanasevich, V. I., Afonin, I. S., Evdokimov, I. O., Mayorov, V. Y., Portnyagin, A. S., Agafonova, I. G., Skurikhina, Y. E., and Medkov, M. A., "Synthetic $CaSiO_3$ sol-gel powder and SPS ceramic derivatives: “In vivo” toxicity assessment", ***Progress In Natural Science: Materials International***, 29 (5): 569–575 (2019).

40. Belokoneva, E. L., Topnikova, A. P., and Aksenov, S. M., "Topolology-symmetry law of structure of natural titanosilicate micas and related heterophyllosilicates based on the extended OD theory: Structure prediction", ***Crystallography Reports***, 60 (1): 1–15 (2015).

41. Hossain, S. S. and Roy, P. K., "Study of physical and dielectric properties of bio-waste-derived synthetic wollastonite", ***Journal Of Asian Ceramic Societies***, 6 (3): 289–298 (2018).

42. Srinath, P., Abdul Azeem, P., and Venugopal Reddy, K., "Review on calcium silicate-based bioceramics in bone tissue engineering", ***International Journal Of Applied Ceramic Technology***, 17 (5): 2450–2464 (2020).

43. Palakurthy, S., K., V. G. R., Samudrala, R. K., and P., A. A., "In vitro bioactivity and degradation behaviour of β-wollastonite derived from natural waste", ***Materials Science And Engineering C***, 98: 109–117 (2019).

44. Anjaneyulu, U. and Sasikumar, S., "Bioactive nanocrystalline wollastonite synthesized by sol-gel combustion method by using eggshell waste as calcium source", 37: 207-212 (2014).

45. Azeena, S., Subhapradha, N., Selvamurugan, N., Narayan, S., Srinivasan, N., Murugesan, R., Chung, T. W., and Moorthi, A., "Antibacterial activity of agricultural waste derived wollastonite doped with copper for bone tissue engineering", ***Materials Science And Engineering C***, 71: 1156–1165 (2017).

46. Zenebe, C, G. "A review on the role of wollastonite biomaterial in bone tissue engineering." ***BioMed Research International*** 2022.1: 4996530 (2022).

47. Ismail, H., and Mohamad, H. Bioactivity and biocompatibility properties of sustainable wollastonite bioceramics from rice husk ash/rice straw ash: A review. *Materials*, *14*(18): 5193 (2021).

48. Ruolan, W., Liangjiao, C., and Longquan, S., "The mTOR/ULK1 signaling pathway mediates the autophagy-promoting and osteogenic effects of dicalcium silicate nanoparticles", ***Journal Of Nanobiotechnology***, 18 (1): 1-19 (2020).

49. Chen, L., Zhang, Y., Liu, J., Wei, L., Song, B., and Shao, L., "Exposure of the murine RAW 264.7 macrophage cell line to dicalcium silicate coating: assessment of cytotoxicity and pro-inflammatory effects", ***Journal Of Materials Science: Materials In Medicine***, 27 (3): 1–11 (2016).

50. Correa, D., Almirall, A., García-Carrodeguas, R., Alberto Dos Santos, L., De Aza, A. H., Parra, J., and Ángel Delgado, J., "β-Dicalcium silicate-based cement: Synthesis, characterization and in vitro bioactivity and biocompatibility studies", ***Journal Of Biomedical Materials Research - Part A***, 102 (10): 3693–3703 (2014).

51. Lai, S., Chen, L., Cao, W., Cui, S., Li, X., Zhong, W., Ma, M., and Zhang, Q., "Dicalcium silicate induced proinflammatory responses through TLR2-mediated NF-κB and JNK pathways in the murine RAW 264.7 macrophage cell line", ***Mediators Of Inflammation***, 2018 (1): 1-16 (2018).

52. Radwan, M. M., Abd El-Hamid, H. K., and Mohamed, A. F., "Influence of saline solution on hydration behavior of β-dicalcium silicate in comparison with biphasic calcium phosphate/hydroxyapatite bio-ceramics", ***Materials Science And Engineering C***, 57: 355–362 (2015).

53. Gou, Z., Chang, J., Zhai, W., and Wang, J., "Study on the self-setting property and the in vitro bioactivity of β-Ca_2SiO_4", ***Journal Of Biomedical Materials Research - Part B Applied Biomaterials***, 73 (2): 244–251 (2005).

54. Chen, C. C., Wang, C. W., Hsueh, N. S., and Ding, S. J., "Improvement of in vitro physicochemical properties and osteogenic activity of calcium sulfate cement for bone repair by dicalcium silicate", ***Journal Of Alloys And Compounds***, 585: 25–31 (2014).

55. Liu, W., Zhai, D., Huan, Z., Wu, C., and Chang, J., "Novel tricalcium silicate/magnesium phosphate composite bone cement having high compressive strength, in vitro bioactivity and cytocompatibility", ***Acta Biomaterialia***, 21: 217–227 (2015).

56. Shi, C., Qian, B., Wang, Q., Zunino, F., Zhao, J., and Shen, X., "Structure analysis of beta dicalcium silicate via scanning transmission electron microscope (STEM)", ***Construction And Building Materials***, 348: 1-12 (2022).

57. Correa, D., Almirall, A., Carrodeguas, R. G., Dos Santos, L. A., De Aza, A. H., Parra, J., Morejon, L., and Delgado, J. A., "α-Tricalcium phosphate cements modified with β-dicalcium silicate and tricalcium aluminate: Physicochemical characterization, in vitro bioactivity and cytotoxicity", ***Journal Of Biomedical Materials Research - Part B Applied Biomaterials***, 103 (1): 72–83 (2015).

58. Li, S. M., Jia, N., Zhu, J. F., Ma, M. G., and Sun, R. C., "Synthesis of cellulose-calcium silicate nanocomposites in ethanol/water mixed solvents and their characterization", ***Carbohydrate Polymers***, 80 (1): 270–275 (2010).

59. Wang, F., Xu, Z., Zhang, Y., Li, J., Nian, S., and Zhou, N., "Green synthesis and bioactivity of vaterite-doped beta-dicalcium silicate bone cement", ***Ceramics International***, 42 (1): 1856–1861 (2016).

60. Wu, B. C., Huang, S. C., and Ding, S. J., "Comparative Osteogenesis of Radiopaque Dicalcium Silicate Cement and White-Colored Mineral Trioxide Aggregate in a Rabbit Femur Model", ***Materials***, 6 (12): 5675–5689 (2013).

61. Ho, C. C., Wei, C. K., Lin, S. Y., and Ding, S. J., "Calcium silicate cements prepared by hydrothermal synthesis for bone repair", ***Ceramics International***, 42 (7): 9183–9189 (2016).

62. Ortaboy, S., Li, J., Geng, G., Myers, R. J., Monteiro, P. J. M., Maboudian, R., and Carraro, C., "Effects of CO_2 and temperature on the structure and chemistry of C-(A-)S-H investigated by Raman spectroscopy", ***RSC Advances***, 7 (77): 48925–48933 (2017).

63. Ding, Z., Xi, W., Ji, M., Li, X., Zhang, Q., and Yan, Y., "The improvement of the self-setting property of the tricalcium silicate bone cement with acid and its mechanism", ***Journal Of Physics And Chemistry Of Solids***, 150: 1-8 (2021).

64. Lin, Q., Zhang, X., Liang, D., Li, J., Wang, W., Wang, Z., and Wong, C. P., "The in vivo dissolution of tricalcium silicate bone cement", ***Journal Of Biomedical Materials Research - Part A***, 109 (12): 2527–2535 (2021).

65. Liu, W. C., Wang, H. Y., Chen, L. C., Huang, S. W., Wu, C., and Chung, R. J., "Hydroxyapatite/tricalcium silicate composites cement derived from novel two-step sol-gel process with good biocompatibility and applications as bone cement and potential coating materials", ***Ceramics International***, 45 (5): 5668–5679 (2019).

66. Zhang, Y., Wu, Z., Shu, Y., Wang, F., Cao, W., and Li, W., "A novel bioactive vaterite-containing tricalcium silicate bone cement by self hydration synthesis and its biological properties", ***Materials Science And Engineering C***, 79: 23–29 (2017).

67. Schamel, M., Barralet, J. E., Groll, J., and Gbureck, U., "In vitro ion adsorption and cytocompatibility of dicalcium phosphate ceramics", ***Biomaterials Research***, 21 (1): 1-8 (2017).

68. Faleh, T, Sheikh, Z and Barralet, J. "Dicalcium phosphate cements: Brushite and monetite." *Acta biomaterialia* 8.2 : 474-487 (2012).

69. Sheikh, Z., Zhang, Y. L., Tamimi, F., and Barralet, J., "Effect of processing conditions of dicalcium phosphate cements on graft resorption and bone formation", ***Acta Biomaterialia***, 53: 526–535 (2017).

70. Shi, X., Zhao, C., Xu, L., and Wang, Q., "Preparation of Dicalcium Phosphate Anhydrous (Monetite) Biological Coating on Titanium by Spray-Drying Method", ***Advances In Materials Science And Engineering***, 2017 (1): 1-7 (2017).

71. Yoo, K. H., Kim, Y. Il, and Yoon, S. Y., "Physicochemical and biological properties of mg-doped calcium silicate endodontic cement", ***Materials***, 14 (8): 1-17 (2021).

72. Xie, L., Luo, D., Zhu, Y., Xu, C., Chen, G. X., Xu, R. J., Zhou, X. Q., and Li, Y., "Monitoring of hydroxyapatite conversion by luminescence intensity and color during mineralization of Sm^{3+}-doped β-dicalcium silicate", ***Journal Of Luminescence***, 226: 1-7 (2020).

73. El-Hamid, H. K. A., Abo-Naf, S. M., and Elwan, R. L., "Characterization, bioactivity investigation and cytotoxicity of borosilicate glass/dicalcium silicate composites", ***Journal Of Non-Crystalline Solids***, 512: 25–32 (2019).

74. Zhang, Y., Wang, D., Wang, F., Jiang, S., and Shu, Y., "Modification of dicalcium silicate bone cement biomaterials by using carboxymethyl cellulose", ***Journal Of Non-Crystalline Solids***, 426: 164–168 (2015).

75. Ho, C. C., Wei, C. K., Lin, S. Y., and Ding, S. J., "Calcium silicate cements prepared by hydrothermal synthesis for bone repair", ***Ceramics International***, 42 (7): 9183–9189 (2016).

76. Dutta, N., and A. Chatterjee. "Hydrothermal synthesis of dicalcium silicate based cement." *IOP Conference Series: Materials Science and Engineering*. Vol. 216. No. 1. IOP Publishing: (1-8) 2017.

77. Zhong, H., Wang, L., Fan, Y., He, L., Lin, K., Jiang, W., Chang, J., and Chen, L., "Mechanical properties and bioactivity of β-Ca_2SiO_4 ceramics synthesized by spark plasma sintering", ***Ceramics International***, 37 (7): 2459–2465 (2011).

78. Mansoor, P. and Dasharath, S. M., "Synthesis and characterization of wollastonite ($CaSiO_3$)/titanium oxide (TiO_2) and hydroxyapatite (HA) ceramic composites for bio-medical applications fabricated by spark plasma sintering technology", *Materials Today: Proceedings*, *45*: 332-337 (2021).

79. Ahmed, M. J., Schollbach, K., van der Laan, S., Florea, M., and Brouwers, H. J. H. A quantitative analysis of dicalcium silicate synthesized via different sol-gel methods. ***Materials & Design***, *213*, 110329: 1-12 (2022).

80. Yunus, S. N. H. M., Fhan, K., F., Johar, B., Adzali, N. M. S., Jakfar, N. H., Ee Meng, C., Mohd Tarmizi, E. Z., and Talib, Z. A., "Effect of sintering temperature on dielectric and electrical properties of bio-waste derived beta-dicalcium silicate", ***Materials Chemistry And Physics***, 309: 1-15 (2023).

81. Gan, Y. X., Jayatissa, A. H., Yu, Z., Chen, X., and Li, M. Hydrothermal synthesis of nanomaterials. *Journal of Nanomaterials*, *2020*: 1-2 (2020).

82. Kumar, D. B., Jerrin, K. A., Joseph, N., & Jiss, A. Review of spark plasma sintering process. In *IOP Conference Series: Materials Science and Engineering*. 933: 1-9 (2020).

83. Dehghanghadikolaei, A., Ansary, J., & Ghoreishi, R. Sol-gel process applications: A mini-review. *Proc. Nat. Res. Soc*, *2*(1): 1-11 (2018).

84. Yang, X., Liu, M., Zhao, Y., Jia, H., Xu, S., Li, X., Chen, X., Zhang, F., Gao, C., and Gou, Z., "Rational design and fabrication of a β-dicalcium silicate-based multifunctional cement with potential for root canal filling treatment", ***Journal Of Materials Chemistry B***, 2 (24): 3830–3838 (2014).

85. Motameni, A., Dalgic, A. D., Alshemary, A. Z., Keskin, D., and Evis, Z., "Structural and Biological Analysis of Mesoporous Lanthanum Doped βTCP For Potential Use as Bone Graft Material", ***Materials Today Communications***, 23: 1-11 (2020).

86. Reller, L. B., Weinstein, M., Jorgensen, J. H., and Ferraro, M. J. Antimicrobial susceptibility testing: a review of general principles and contemporary practices. *Clinical infectious diseases*, *49*(11): 1749-1755 (2009).

87. Liu, W., Huan, Z., Xing, M., Tian, T., Xia, W., Wu, C., Zhou, Z., and Chang, J., "Strontium-substituted dicalcium silicate bone cements with enhanced osteogenesis potential for orthopaedic applications", ***Materials***, 12 (14): (2019).

88. Gou, Z. and Chang, J., "Synthesis and in vitro bioactivity of dicalcium silicate powders", ***Journal Of The European Ceramic Society***, 24 (1): 93–99 (2004).

89. Timón, V., Torrens-Martin, D., Fernández-Carrasco, L. J., and Martínez-Ramírez, S., "Infrared and Raman vibrational modelling of β-C_2S and C_3S compounds", ***Cement And Concrete Research***, 169: 1-11(2023).

90. Yunus, S. N. H., Fhan, K. S., Johar, B., Adzali, N. M. S., Jakfar, N. H., Meng, C. E., ... and Talib, Z. A. Formation of Bio-based Derived Dicalcium Silicate Ceramics via Mechanochemical Treatment: Physical, XRD, SEM and FTIR Analyses. *International Journal of Nanoelectronics & Materials*, *16*(3): 1-19 (2023).

91. Chrysafi, R., Perraki, T., and Kakali, G., "Sol-gel preparation of $2CaO \cdot SiO_2$", ***Journal Of The European Ceramic Society***, 27 (2–3): 1707–1710 (2007).

92. Balbinot, G. de S., Leitune, V. C. B., Nunes, J. S., Visioli, F., and Collares, F. M., "Synthesis of sol–gel derived calcium silicate particles and development of a bioactive endodontic cement", ***Dental Materials***, 36 (1): 135–144 (2020).

93. Guo, X., Long, Y., Li, W., and Dai, H., "Osteogenic effects of magnesium substitution in nano-structured β-tricalcium phosphate produced by microwave synthesis", ***Journal Of Materials Science***, 54 (16): 11197–11212 (2019).

94. Grigoraviciute-Puroniene, I., Tsuru, K., Garskaite, E., Stankeviciute, Z., Beganskiene, A., Ishikawa, K., and Kareiva, A., "A novel wet polymeric precipitation synthesis method for monophasic β-TCP", ***Advanced Powder Technology***, 28 (9): 2325–2331 (2017).

95. Taha, A., Akram, M., Jawad, Z., Alshemary, A. Z., and Hussain, R., "Strontium doped injectable bone cement for potential drug delivery applications", ***Materials Science And Engineering C***, 80: 93–101 (2017).

96. Mirhadi, B., Mehdikhani, B., & Askari, N. Synthesis of nano-sized β-tricalcium phosphate via wet precipitation. Processing and Application of Ceramics, 5(4): 193-198 (2011).

97. Yao, C., Pripatnanont, P., Zhang, J., and Suttapreyasri, S., "Fabrication and characterization of a bioactive composite scaffold based on polymeric collagen/gelatin/nano β-TCP for alveolar bone regeneration", ***Journal Of The Mechanical Behavior Of Biomedical Materials***, 135: 106500 (2024).

98. Alshemary, A. Z., Bilgin, S., Işık, G., Motameni, A., Tezcaner, A., and Evis, Z., "Biomechanical Evaluation of an Injectable Alginate / Dicalcium Phosphate Cement Composites for Bone Tissue Engineering", ***Journal Of The Mechanical Behavior Of Biomedical Materials***, 118: 1-11 (2021).

99. Gandou, Z., Nounah, A., Nouneh, K., and Yahyaoui, A., "Effect of time of microwave activation synthesis on crystallite size of spheroid β Tricalcium Phosphate nanopowders", ***J. Mater. Environ. Sci***, 7 (5): 1653–1662 (2016).

100. Coelho, P. G., Coimbra, M. E., Ribeiro, C., Fancio, E., Higa, O., Suzuki, M., and Marincola, M., "Physico/chemical characterization and preliminary human histology assessment of a β-TCP particulate material for bone augmentation", ***Materials Science And Engineering C***, 29 (7): 2085–2091 (2009).

101. Massit, A., El Yacoubi, A., Hmamouchi, S., Rkhaila, A., Boulouiz, A., Ounine, K., and El Idrissi, B. C., "Sulphate-substituted tricalcium phosphate β-TCP: Effect of SO_4^{-2} insertion and microwave conditions", ***Materials Today: Proceedings***, 72: 3544–3549 (2023).

102. Xie, L., Yu, H., Deng, Y., Yang, W., Liao, L., and Long, Q., "Preparation, characterization and in vitro dissolution behavior of porous biphasic α/β-tricalcium phosphate bioceramics", ***Materials Science And Engineering C***, 59: 1007–1015 (2016).

103. Raynaud, S., Champion, E., Bernache-Assollant, D., & Thomas, P. Calcium phosphate apatites with variable Ca/P atomic ratio I. Synthesis, characterisation and thermal stability of powders. *Biomaterials*, *23*(4): 1065-1072 (2002).

104. Mirjalili, F., Mohammadi, H., Azimi, M., Hafezi, M., and Abu Osman, N. A., "Synthesis and characterization of β-TCP/CNT nanocomposite: Morphology, microstructure and in vitro bioactivity", ***Ceramics International***, 43 (10): 7573–7580 (2017).

105. Liu, S., Dou, Z., Zhang, S., Zhang, H., Guan, X., Feng, C., and Zhang, J., "Effect of sodium hydroxide on the carbonation behavior of β-dicalcium silicate", ***Construction And Building Materials***, 150: 591–594 (2017).

106. Alshemary, A. Z., Goh, Y. F., Akram, M., Razali, I. R., Abdul Kadir, M. R., and Hussain, R., "Microwave assisted synthesis of nano sized sulphate doped hydroxyapatite", ***Materials Research Bulletin***, 48 (6): 2106–2110 (2013).

107. Ahmed, M. J., Lambrechts, K., Ling, X., Schollbach, K., and Brouwers, H. J. H., "Effect of hydroxide, carbonate, and sulphate anions on the β-dicalcium silicate hydration rate", ***Cement And Concrete Research***, 173: 1-10 (2023).

108. Alshemary, A. Z., Bilgin, S., Işık, G., Motameni, A., Tezcaner, A., and Evis, Z., "Biomechanical Evaluation of an Injectable Alginate / Dicalcium Phosphate Cement Composites for Bone Tissue Engineering", ***Journal Of The Mechanical Behavior Of Biomedical Materials***, 118: 1-11 (2021).

109. Liu, W., Huan, Z., Xing, M., Tian, T., Xia, W., Wu, C., Zhou, Z., and Chang, J., "Strontium-substituted dicalcium silicate bone cements with enhanced osteogenesis potential for orthopaedic applications", ***Materials***, 12 (14): 1-16 (2019).

110. Radwan, M. M., Abd El-Hamid, H. K., and Mohamed, A. F., "Influence of saline solution on hydration behavior of β-dicalcium silicate in comparison with biphasic calcium phosphate/hydroxyapatite bio-ceramics", ***Materials Science And Engineering C***, 57: 355–362 (2015).

111. Elreash, A. A., Hamama, H., Eldars, W., Lingwei, G., Zaen El-Din, A. M., and Xiaoli, X., "Antimicrobial activity and pH measurement of calcium silicate

cements versus new bioactive resin composite restorative material", ***BMC Oral Health***, 19 (1): 1-10 (2019).

112. Santiago, M. C., Gomes-Cornélio, A. L., de Oliveira, L. A., Tanomaru-Filho, M., and Salles, L. P., "Calcium silicate-based cements cause environmental stiffness and show diverse potential to induce osteogenesis in human osteoblastic cells", ***Scientific Reports***, 11 (1): 1-11 (2021).

113. Berridge, M. J., Lipp, P., and Bootman, M. D., "The versatility and universality of calcium signalling", ***Nature Reviews Molecular Cell Biology***, 1 (1): 11–21 (2000).

114. Bootman, M. D. and Bultynck, G., "Fundamentals of cellular calcium signaling: A primer", ***Cold Spring Harbor Perspectives In Biology***, 12 (1): 1-18 (2020).

115. Orrenius, S., Zhivotovsky, B., and Nicotera, P., "Regulation of cell death: the calcium–apoptosis link", ***Nature Reviews Molecular Cell Biology***, 4 (7): 552–565 (2003).

RESUME

Mohamed ALHELEBU graduated from the Department of Chemical Engineering at the International University of Sham in 2020. He started his master's program in the Department of Biomedical Engineering at Karabuk University in 2021.